The sustainability of geothermal energy in an aquifer

A mathematical model

Merijn Jellema

TU Delft

March 24, 2025

The sustainability of geothermal energy in an aquifer

Jellema, M.

TU Delft, Bachelor Applied Physics and Mathematics

Meulenbroek, Dr. B.J.

TU Delft, Applied Mathematics

Bera, Dr. B.

TU Delft, Applied Physics
B.Bera@tudelft.nl

March 24, 2025

Abstract

Geothermal energy plays a role in advancing clean energy solutions for a sustainable future, which is why we investigate the sustainability of geothermal systems in an aquifer. The geothermal system examined in this research operates using two wells, positioned 1 km apart. One well pumps cold water into the porous medium and the second well pumps warm water out of the aquifer. As warm water is extracted, the temperature of the aquifer decreases. This cooling disturbs the chemical balance of the minerals in the water, which can lead to precipitation reactions. This precipitation reduces the porosity and consequently the permeability of the aquifer.

The temperature distribution is modeled using the pressure and velocity field. This showed that the aquifer had cooled to $40°C$ in 6 years. According to this result, the use of a geothermal aquifer is not sustainable. The cooling within 6 years is not accurate, because the boundary conditions that were selected were not fully chosen to reflect the complexities of the system and we didn't properly consider the heat coming from Earth's core.

Precipitation reactions lead to an increase or decrease in concentration of various minerals in the water. These reactions cause deposits of solid minerals on the grains or porous rock, causing the aquifer to clog, allowing less and less water to flow through. In this model, the amount of precipitation was very small and therefore had little effect on the water flow and the sustainability of the aquifer.

Contents

List of symbols

Variable	Symbol	Value	Unit
Length of the aquifer	L	1000 [1]	m
Width of the aquifer	H	1000	m
Thickness of the aquifer	τ	30 [2]	m
Injection flux	Q_{inj}	300 [2]	$\frac{m^3}{hr}$
		0.083	$\frac{m^3}{s}$
Initial porosity	ϕ_0	0.15 [2]	-
Flow rate	u_0	$3.17 \cdot 10^{-5}$ [2]	$\frac{m}{s}$
Initial permeability	k_0	10^{-12}	m^2
Viscosity of water	μ	$1.1375 \cdot 10^{-3}$[3]	$Pa \cdot s$
Characteristic distance	d_c	1000	m
Characteristic time	t_c	$5.4 \cdot 10^7$	s
Characteristic velocity	u_c	$1.85 \cdot 10^{-5}$	$\frac{m}{s}$
Characteristic pressure	p_c	$21 \cdot 10^6$	Pa
Thermal conductivity water	λ_w	0.6 [3]	$\frac{W}{m \cdot K}$
Density water	ρ_w	$1 \cdot 10^3$ [3]	$\frac{kg}{m^3}$
Specific heat water	c_w	$4.18 \cdot 10^3$ [3]	$\frac{J}{kg \cdot K}$
Thermal conductivity porous medium	λ_{pm}	1.1 [3]	$\frac{W}{m \cdot K}$
Density porous medium	ρ_{pm}	$2.6 \cdot 10^3$ [3]	$\frac{kg}{m^3}$
Specific heat porous medium	c_{pm}	$0.8 \cdot 10^3$ [3]	$\frac{J}{kg \cdot K}$
Low temperature	T_{low}	15	$^\circ C$
High temperature	T_{high}	80 [4]	$^\circ C$
Diffusion coefficient	$\mathcal{D}$	$1.5 \cdot 10^{-9}$ [5]	$\frac{m^2}{s}$
Arrhenius pre-exponential factor	A	$4.65 \cdot 10^{-2}$ [2]	$\frac{1}{m^2 s}$
Activation energy	E_a	34000 [2]	$\frac{J}{mol}$
Universal gas constant	R	8314.3	$\frac{J}{mol \cdot K}$
Reactive surface area	$A_{diss} = A_{prec}$	1	$\frac{m^2}{kg}$
Initial concentration of the porous medium	C_{pm}	$2 \cdot 10^{-4}$	$\frac{mol}{kgw}$
Initial concentration of Na^+	C_{Na^+}	$1.84 \cdot 10^{-1}$ [2]	$\frac{mol}{kgw}$
Initial concentration of Cl^-	C_{Cl^-}	$4 \cdot 10^{-3}$ [2]	$\frac{mol}{kgw}$
Activity coefficient for Na^+	γ_{Na^+}	$1.188 \cdot 10^{-1}$[2]	-
Activity coefficient for Cl^-	γ_{Cl^-}	$2.659 \cdot 10^{-3}$ [2]	-
Step size in the x-direction	Δx	0.01	m
Step size in the y-direction	Δy	0.01	m

Table 1: An overview of all the parameters used in this model.

Introduction

Geothermal energy is a renewable energy source derived from the internal heat of the Earth. It harnesses thermal energy generated and stored within the Earth's crust. Unlike fossil fuels, geothermal energy is environmentally friendly, producing minimal greenhouse gas emissions. With its reliability and low operational costs, geothermal energy plays an increasing role in the advancement of clean energy solutions for a sustainable future. In 2022, geothermal energy contributes approximately 0.5% to the global electricity generation capacity [6]. The Dutch government aims to increase this share, targeting geothermal energy to meet 5% of the nation's heating demand by 2030 and 23% by 2050 [7].

Geothermal aquifers are natural underground reservoirs of water heated by the internal heat of the Earth. These aquifers, located within permeable rock formations, serve as a key source of geothermal energy. The water in these aquifers absorbs heat from the surrounding rocks, often reaching high temperatures. By tapping into these geothermal aquifers, we can extract heat for various applications such as electricity generation, direct heating systems and agricultural uses.

The geothermal system examined in this research operates using two wells, positioned 1 km apart (Figure 1.1). One well pumps cold water into the porous medium and the second well pumps warm water out of the aquifer.

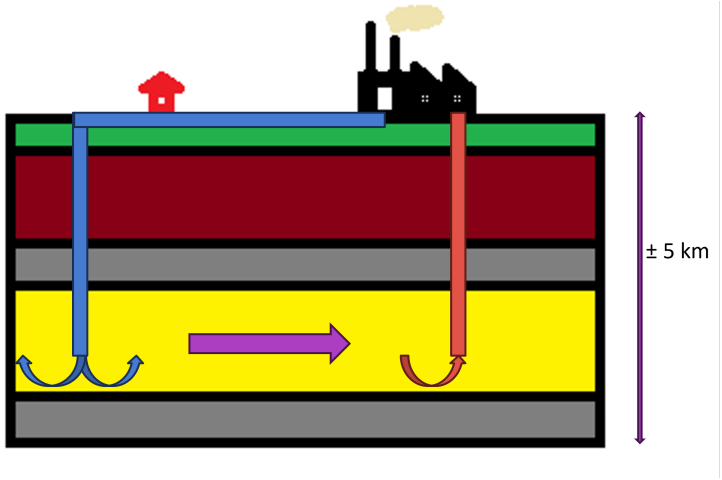

Figure 1.1: Geothermal system with an aquifer at several kilometers deep where the temperature is around 80 °C. The aquifer (yellow) is enclosed by two layers with a low permeability (gray). The left well (blue) pumps water into the aquifer and the right well (red) pumps heated water out of the aquifer.

As warm water is extracted, the temperature of the aquifer decreases. This cooling disturbs the chemical balance of the minerals in the water, which can lead to precipitation reactions. This precipitation reduces the porosity and, consequently, the permeability. As a result, the pumps that circulate water in and out of the aquifer must work harder, increasing energy consumption. Eventually, the energy required for pumping may exceed the amount of energy extracted from the water. We would like to prevent this from happening and have a better understanding of these processes by modeling the relation between porosity, permeability and reaction rate.

Therefore, our main research question:

How sustainable is the use of geothermal energy in an aquifer?

We divide this research question into two subquestions:

How long does it take for the geothermal aquifer to cool?

How long does it take for the geothermal aquifer to clog due to precipitation reactions?

Derivation of the model equations

This chapter will cover the geometric domain and system used in this model (section 2.1), the properties of the porous medium (section 2.2), the Darcy model (section 2.3) and the dimensionless quantities used in this model (section 2.4). We will also formulate the model equations for the pressure/velocity field (section 2.5), the temperature distribution (section 2.6) and the concentration field (section 2.7).

2.1 Geometric domain

An enclosed aquifer located several kilometers beneath the surface will be examined, focusing on a two-dimensional horizontal domain characterized by a length $x = L$ and a width $y = H$ (see Figure 2.1).

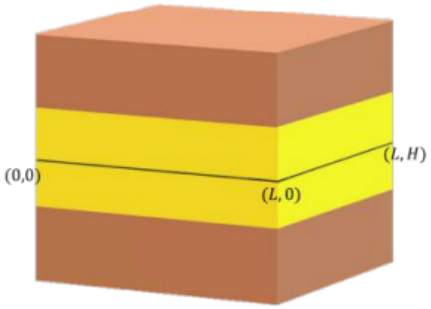

Figure 2.1: Schematic representation of an aquifer (yellow) enclosed by two layers with a low permeability (brown) with dimensions L x H. [8]

In general, in a geothermal system, two cylindrical wells are placed, with the water flowing radially. This water is slowly heated by the porous medium as the water flows further. Some of this heated water is pumped up through the other well (see Figure 2.2a).
In this model, the geothermal system has been simplified in two ways:

1. We set the well width to match the domain width. Due to the chosen control volume (Lx H), the curvatures in the flow pattern are negligible. Instead of a circular flow pattern, this results in a parallel flow pattern. This simplifies the model since there's no need to use cylindrical coordinates.

2. We assume that all the water flows directly from one well to the other in a parallel manner.

With this simplification we lose accuracy, because in a circular flow pattern, the velocity and therefore the pressure decreases as the water flows further. This is not the case with the simplification. These simplifications lead to the simplified geothermal model depicted in Figure 2.2b.

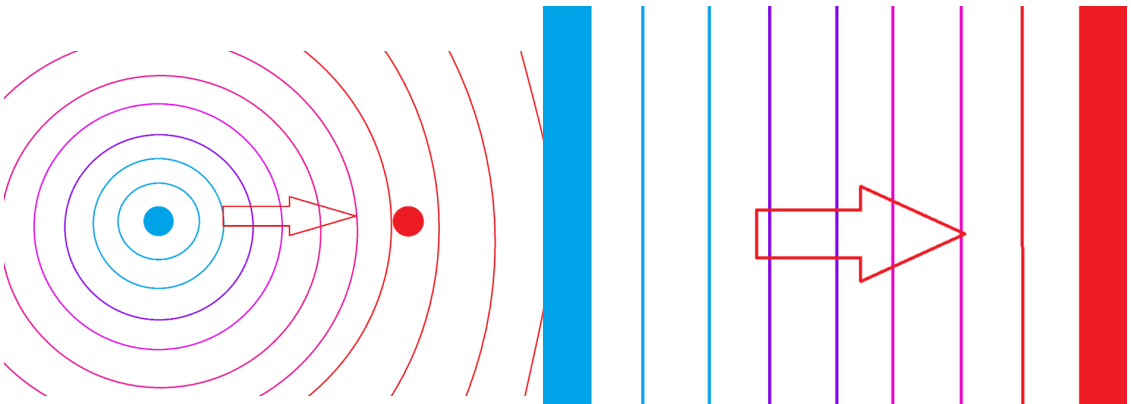

(a) A general geothermal system with two cylindrical wells where water with a low temperature flows in a circular manner out of the (blue) well. This water is slowly heated by the porous medium as the water flows further. Some of this heated water is pumped up through the other (red) well.

(b) The simplified geothermal model used in this model with a parallel flow pattern and the width of the wells match the domain width.

Figure 2.2: Top view of two geothermal systems: a general system on the left and the applied model on the right. The color gradient from blue to red represents the increase in water temperature. The arrow indicates the relevant direction of water flow.

2.2 Properties of the porous medium

The aquifer is composed of a porous medium saturated with water and has two important characteristics. The first characteristic is the porosity ϕ, which indicates the fraction of the total volume that is occupied by water. The second characteristic is the permeability k, which is a measure of how easily the water can flow through the pores of the medium (Figure 2.3). The permeability is influenced by the structure, the size of grains in the porous medium and by precipitation due to chemical reactions on the grains.

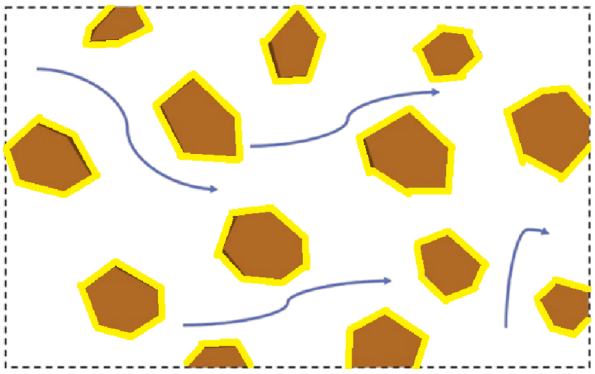

Figure 2.3: Schematic representation of the porous medium in the aquifer. The precipitation (yellow) on the grains (brown) causes the water to flow less smoothly through the pores (white). The arrows represent possible flow paths of water through the medium.

2.3 The Darcy model

In this project we consider velocities of the water in a porous medium at a macroscopic scale, the Darcy velocity. The superficial velocity is calculated by dividing the water flux passing through a cross-section of the medium by the area of that cross-section. Due to the partial coverage of this region with a porous medium, the Darcy velocity is less than the actual velocity. In this model, we will

simulate two extremely wide wells with a water flow that is parallel and flows from one well to the other.

Darcy's law is an equation that describes the flow of a fluid through a porous medium. This law states that velocity is proportional to pressure gradient and is given by:

$$\overrightarrow{u} = -\frac{k}{\mu}\nabla p \tag{2.1}$$

with Darcy velocity $\overrightarrow{u}$, permeability k, viscosity μ and pressure p. The Darcy velocity is a superficial velocity that is given as the volume flow rate over a chosen area and is different from the local velocity in the porous medium. The Darcy velocity is a velocity field that only gives the general direction and speed. The Darcy model can only be applied if the Reynolds number is very low, which is the case in this model.

2.4 Dimensionless quantities

Each dimensionless quantity relates to a specific problem. In this case, we are focused on the interactions and dynamics occurring between the two wells within the macroscopic model of a geothermal system. Therefore, the following quantities are normalized:

$$x_d = \frac{x}{d_c} \tag{2.2}$$

$$y_d = \frac{y}{d_c} \tag{2.3}$$

With $d_c = L = 1000\ m$ the distance between the two wells. x is the horizontal axis of the domain (from 0 to L) and y is the vertical axis of the domain (from 0 to H).

Now for the dimensionless quantity time t_d, we use the "porevolume", as follows

$$t_d = \frac{t}{t_c} \tag{2.4}$$

With $t_c = \frac{L\tau H\phi_0}{Q_{inj}} = 5.4 \cdot 10^7\ s \approx 1.7$ years, where $Q_{inj} = 0.083\ \frac{m^3}{s}$ is the injection flux, $\phi_0 = 0.15$ is the initial porosity, $H = 1000\ m$ the width of the porous medium and $\tau = 30\ m$ the thickness of the porous medium. In this case, $t = t_c$ is the time it takes to fill up the porous medium with water.

The dimensionless velocity u_d is calculated using the d_c and t_c, as follows

$$u_d = \frac{u}{u_c} \tag{2.5}$$

With $u_c = \frac{d_c}{t_c} = \frac{Q_{inj}}{\tau H\phi} = 1.85 \cdot 10^{-5}\ \frac{m}{s} \approx 1.6\ \frac{m}{day}$.

To get the dimensionless quantity for pressure p_d, we use Darcy's law in 1D and the dimensionless x_d and u_d.

$$\begin{aligned} u &= -\frac{k_0}{\mu}\nabla p \\ u_d \cdot u_c &= -\frac{k_0}{\mu}\frac{dp_d \cdot p_c}{dx_d \cdot d_c} \\ u_d &= -\frac{k_0 p_c}{\mu d_c u_c}\frac{dp_d}{dx} \\ \frac{k_0 p_c}{\mu d_c u_c} &= 1 \\ p_c &= \frac{\mu d_c u_c}{k_0} \end{aligned} \tag{2.6}$$

With $\mu = 1.1375 \cdot 10^{-3}\ Pa \cdot s$ is the viscosity of water and $k_0 = 10^{-12}\ m^2$ the initial permeability. So we get a dimensionless quantity p_d:

$$p_d = \frac{p}{p_c} \tag{2.7}$$

With $p_c = \frac{\mu L Q_{inj}}{k_0 \tau H \phi_0} \approx 21 \cdot 10^6\ Pa = 21$ Bar.

For the dimensionless quantity temperature T_d, we have

$$T_d = \frac{T - T_{low}}{T_{high} - T_{low}} \tag{2.8}$$

Where T_{low} is the temperature of the cold water that is pumped into the porous medium and T_{high} the temperature of the porous medium at $t = 0$.

For the concentration of two dissolved substances, we assume that one of the substances is in abundance, we have

$$C_d = \frac{C - C_{pm}}{C_{pm}} \tag{2.9}$$

With $C_{pm} = \frac{K_{eq}(T_{high})}{\gamma_{Cl^-}\gamma_{Na^+}C_{Na^+}} = 2 \cdot 10^{-4}\frac{mol}{kgw}$ the initial concentration of the porous medium (see equation 2.40).

2.5 Conservation of mass

The law of conservation of mass states that for any closed system, the mass of the system must remain constant over time. In this case, no water should appear or disappear when flowing through the porous medium. This is shown by the following equation:

$$m = \iiint_{\Delta V} \rho\phi dV \tag{2.10}$$

Where m is the mass, ΔV a small volume where the water flows though, ρ the density of water and ϕ the porosity, the fraction of the volume that is occupied by water.
The mass flow Φ is defined as the amount of water that flows into the system per time given by the formula:

$$\Phi = -\oiint_S (\rho \overrightarrow{u}) \cdot \hat{n} dS = -\iiint_{\Delta V} \nabla \cdot (\rho \overrightarrow{u}) dV \tag{2.11}$$

Here the divergence theorem is applied after the second equal sign A.1.
The change in total mass is only due to mass flow. So by differentiating m with respect to time, as follows

$$\frac{dm}{dt} = \frac{d}{dt}\iiint_{\Delta V} \rho\phi dV = \iiint_{\Delta V} \frac{d}{dt}\rho\phi dV = -\iiint_{\Delta V} \nabla \cdot (\rho \overrightarrow{u}) dV = \Phi \tag{2.12}$$

From this expression we extract:

$$\frac{\partial}{\partial t}(\rho\phi) = -\nabla \cdot (\rho \overrightarrow{u}) \tag{2.13}$$

In this model we look at a parallel water flow from one well to the other. So we assume that water flows in at $x = 0$ with velocity u_0 and out at $x = L$ with the same velocity. We also assume that there is no water flow in or out of the boundaries at $y = 0$ and $y = H$, because the only water inflow is at the boundary $x = 0$ and de flow pattern is parallel (see Figure 2.4).

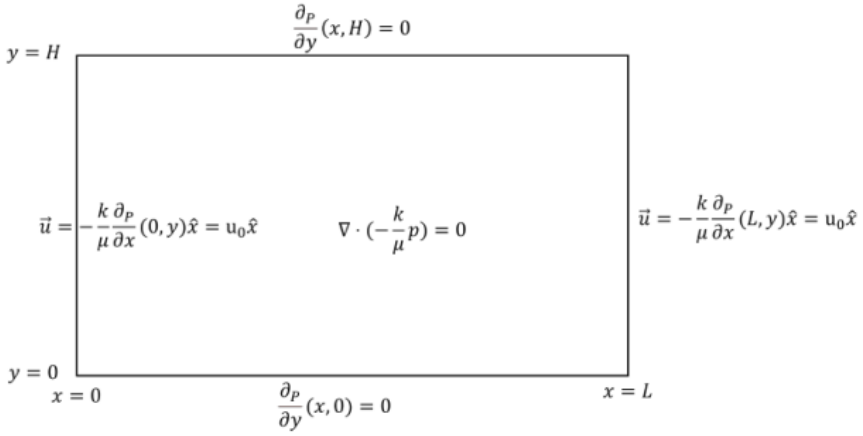

Figure 2.4: Visual representation of the equation and the boundary conditions for the pressure field p. Through the boundaries $x = 0$ and $x = L$ we have a water flow of u_0. Using the law of Darcy, we get the boundary condition $-\frac{k}{\mu}\frac{\partial p}{\partial x}(0/L, y)\hat{x} = u_0\hat{x}$. We also assume that there is no water flow through the boundaries at $y = 0$ and $y = H$ [8]. Using the law of Darcy again, we get $\frac{\partial p}{\partial y}(x, 0/H) = 0$.

If we assume that ρ and ϕ are constant over time and space (later, we assume that ϕ is a function of time, because of precipitation reactions, see section 3.3), as follows

$$\begin{cases} \nabla \cdot \overrightarrow{u} = 0 \\ \overrightarrow{u} = -\frac{k}{\mu}\nabla p \\ \overrightarrow{u}(x,0) = \overrightarrow{u}(x,H) = -\frac{k}{\mu}\frac{\partial p}{\partial y}(x,0) = -\frac{k}{\mu}\frac{\partial p}{\partial y}(x,H) = 0 \\ \overrightarrow{u}(0,y) = \overrightarrow{u}(L,y) = -\frac{k}{\mu}\frac{\partial p}{\partial x}(0,y) = -\frac{k}{\mu}\frac{\partial p}{\partial x}(L,y) = u_0 \end{cases} \tag{2.14}$$

Now we substitute Darcy's law in 2.14 and we get our pressure field equation with boundary conditions:

$$\begin{cases} \nabla \cdot (-\frac{k}{\mu}\nabla p) = 0 \\ \frac{\partial p}{\partial y}(x,0) = \frac{\partial p}{\partial y}(x,H) = 0 \\ \frac{\partial p}{\partial x}(0,y) = -\frac{u_0}{\frac{k}{\mu}(0,y)} \\ \frac{\partial p}{\partial x}(L,y) = -\frac{u_0}{\frac{k}{\mu}(L,y)} \end{cases} \tag{2.15}$$

And this equation in dimensionless form:

$$\nabla \cdot (-\frac{k}{\mu}p_c\nabla p_d) = 0 \tag{2.16}$$

2.6 Temperature

There are three ways of heat transport: diffusion/conduction, convection and radiation. In this model we will only look at diffusion and convection, because the radiation of heat is negligible.
First we define a heat energy density e, which is linearly related to the temperature T:

$$e(x,y,t) = c_w\rho T(x,y,t) \tag{2.17}$$

The specific heat for water c_w can be considered a constant in the model's temperature range.
The convection flux density $\overrightarrow{\Phi_c}$ refers to the rate at which heat is transferred by convection per unit area and is given by:

$$\overrightarrow{\Phi_c} = e\overrightarrow{u} = c_w\rho T\overrightarrow{u} \tag{2.18}$$

The diffusion flux density $\overrightarrow{\hat{\Phi}_d}$ relates to the Fourier's law given by:

$$\overrightarrow{\hat{\Phi}_d} = -\lambda \nabla T \tag{2.19}$$

with λ the thermal conductivity.

The changes in heat energy density caused by the diffusion and convection flux are calculated using the divergence theorem applied to a small volume ΔV.

$$\Delta V \phi \frac{\partial e}{\partial t} = -\oint_S \overrightarrow{\hat{\Phi}_d} \cdot \hat{n} dS - \oint_S c_w \rho T \overrightarrow{u} \cdot \hat{n} dS = -\iint_{\Delta V} \nabla \cdot \overrightarrow{\hat{\Phi}_d} dV - \iint_{\Delta V} \nabla \cdot (c_w \rho T \overrightarrow{u}) dV = \Delta V (\lambda \nabla^2 T - c_w \rho \nabla \cdot (T \overrightarrow{u})) \tag{2.20}$$

From this expression we extract:

$$\frac{\partial T}{\partial t} = \frac{1}{c_w \rho} \frac{\partial e}{\partial t} = \frac{a}{\phi} \nabla^2 T - \frac{1}{\phi} \nabla \cdot (T \overrightarrow{u}) \tag{2.21}$$

with thermal diffusivity $a = \frac{\lambda}{c_w \rho}$.

The sand will cool rapidly in comparison to the duration required for water to flow around the grains [8] [9] [10]. Consequently, the temperatures of both the porous medium T_{pm} and the water T_w can be considered approximately equal, represented as T. However, the heat diffusivity coefficients of the two materials are not identical, leading us to formulate two distinct heat equations: one for the temperature of the water (see equation A.2) and another for the temperature of the medium (see equation A.3). Then we get the complete heat equation with both the porous medium and water parameters, as follows

$$\frac{\partial T}{\partial t} = \frac{\lambda_w + \lambda_{pm}}{c_w \rho_w \phi + c_{pm} \rho_{pm} (1 - \phi)} \nabla^2 T - \frac{c_w \rho_w}{c_w \rho_w \phi + c_{pm} \rho_{pm} (1 - \phi)} \nabla \cdot (T \overrightarrow{u}) =: \alpha \nabla^2 T - \beta \nabla \cdot (T \overrightarrow{u}) \tag{2.22}$$

where we defined an effective thermal diffusivity α and the correction factor for convective heat transport β. See A.2 for the steps between equation 2.21 and 2.22.

For this model we assume that at x=0, water is pumped in with a temperature T_{low}. At $x > 0$ the initial temperature of the porous medium is T_{high}. We also assume that there is no heat transfer at the boundaries $y = 0$ and $y = H$, because the domain repeats itself for higher and lower values of y. We intoduce the Péclet number $\frac{\beta u \Delta x}{\alpha}$, where α and β are the coefficients of equation 2.22, u the velocity of the fluid flow and Δx the step size used in the model. Calculating the Péclet number, we see that the heat transport is dominated by convection. Therefore we set the boundary at $x = L$ to have no heat diffusion, assuming that diffusion is not an important contributor to heat flow at this location.

This gives the following boundary and initial conditions:

$$\begin{cases} T(0, y, t) = T_{low} \\ \frac{\partial T}{\partial x}(L, y, t) = 0 \\ \frac{\partial T}{\partial y}(x, 0, t) = 0 \\ \frac{\partial T}{\partial y}(x, H, t) = 0 \\ T(x > 0, y, 0) = T_{high} \end{cases} \tag{2.23}$$

And this equation in dimensionless form:

$$\frac{\partial T_d}{\partial t_d} = \alpha \frac{t_c}{d_c} \nabla^2 T_d - \beta \frac{t_c u_c}{d_c} \nabla \cdot (T_d \overrightarrow{u_d}) \tag{2.24}$$

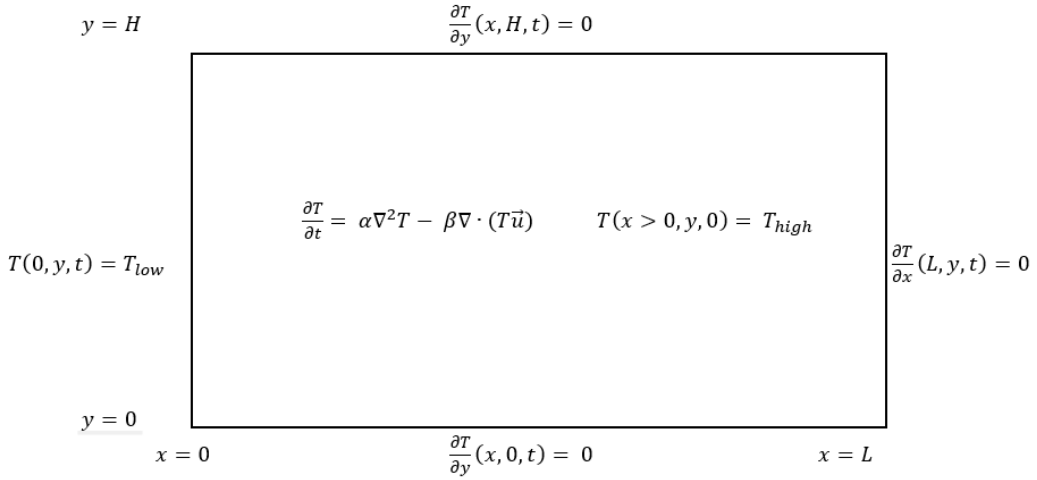

Figure 2.5: Visual representation of equation and the boundary conditions for the temperature distribution T. At the boundaries $y = 0$ and $y = H$ there is no heat transfer, because the domain repeats itself for higher and lower values of y. At $x = L$ to have no heat diffusion, because the heat transport is dominated by convection. At $x = 0$, water is pumped in with a temperature T_{low}. At $x > 0$ the initial temperature of the porous medium is T_{high}.

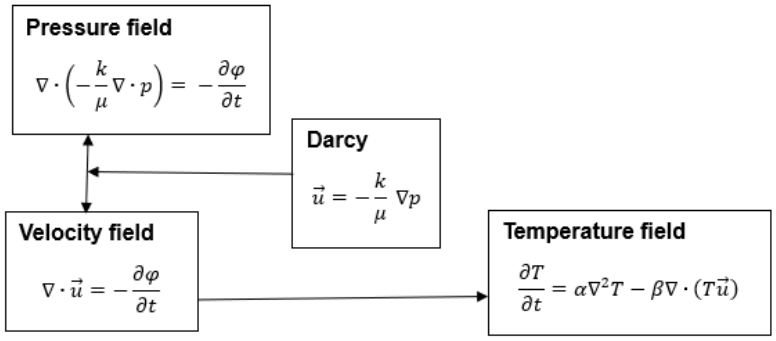

Figure 2.6: The schematic representation of the model derived thus far.

2.7 Concentration

The change in concentration C of dissolved substances in the water depends on diffusion, convection and potential reactions with other materials. The calculations for the concentrations are similar to those of the temperature. Only here Fourier's law is replaced by Fick's law for diffusion ánd there is a reaction rate term r. The convection flux density $\overrightarrow{q_c}$ is given by:

$$\overrightarrow{q_c} = C\overrightarrow{u} \tag{2.25}$$

And the diffusion flux density $\overrightarrow{q_d}$ is given by:

$$\overrightarrow{q_d} = -\mathcal{D}\nabla C \tag{2.26}$$

with the diffusivity $\mathcal{D}$. Using the divergence theorem we get he change in concentration inside a small volume ΔV.

$$\Delta V\phi\frac{\partial C}{\partial t} = -\oint_S(\overrightarrow{q_d}+\overrightarrow{q_c})\cdot\hat{n}dS - r\phi\Delta V = -\iint_{\Delta V}\nabla\cdot(-\mathcal{D}\nabla C + C\overrightarrow{u})dV - r\phi\Delta V = \Delta V(\mathcal{D}\nabla^2 C - \nabla\cdot(C\overrightarrow{u}) - r\phi) \tag{2.27}$$

And simplifying this gives the model equation for the concentration of species A:

$$\frac{\partial C}{\partial t} = \frac{\mathcal{D}}{\phi}\nabla^2 C - \frac{1}{\phi}\nabla\cdot(C\overrightarrow{u}) - r \tag{2.28}$$

We assume that there is no flux of dissolvents at the boundaries $y = 0$ and $y = h$. At $x = 0$ the concentration is given by the injection concentration C_{in}. The initial concentration of the porous medium is given by C_{pm}.

$$\begin{cases} C(0,y,t) = C_{in} \\ \frac{\partial C}{\partial x}(L,y,t) = 0 \\ \frac{\partial C}{\partial y}(x,0,t) = 0 \\ \frac{\partial C}{\partial y}(x,H,t) = 0 \\ C(x>0,y,0) = C_{pm} \end{cases} \tag{2.29}$$

2.7.1 Precipitation reactions

Precipitation reactions are chemical reactions in which two soluble reactants combine in an aqueous solution to form an insoluble solid, called a precipitate. This occurs when the product of the reaction exceeds the solubility limit of a compound. Precipitation reactions are typically represented by double displacement equations and are used in qualitative analysis to identify ions in a solution.

We determine the reactionrate/net precipitation rate r by considering a precipitation reaction with two species A and B:

$$AB \leftrightarrow A + B \tag{2.30}$$

The activity related to the concentration of a species A (similarly for species B) is defined as

$$a_A = \frac{\gamma_A C_A}{\gamma_r C_r} \tag{2.31}$$

Where γ_A is the activity coefficient and C_A the concentration of species A. The reference concentration C_r and the reference activity coefficient γ_r are both chosen to be one.

The precipitation rate R_{prec} (backward arrow) is given by

$$R_{prec} = A_{prec}k_{prec}a_A a_B = A_{prec}k_{prec}IAP \tag{2.32}$$

Here a_A and a_B are the activities related to the concentration of respectively species A and B, A_{prec} the surface area (in m^2) and k_{prec} the precipitation reaction constant. The ionic activity product (IAP) is defined as

$$IAP = a_A a_B = \frac{\gamma_A\gamma_B C_A\cdot C_B}{\gamma_r^2 C_r^2} \tag{2.33}$$

The dissolution rate R_{diss} (forward arrow) is given by

$$R_{diss} = A_{diss}k_{diss} \tag{2.34}$$

The activity of a solid is assumed to be one.

The net precipitation rate r is given by

$$r = R_{prec} - R_{diss} = A_{diss}k_{diss}\left(\frac{IAP}{K_{eq}} - 1\right) \tag{2.35}$$

Where the equilibrium constant K_{eq} is defined as

$$K_{eq} = \frac{A_{diss} k_{diss}}{A_{prec} k_{prec}} \tag{2.36}$$

Since k_{prec} is difficult to determine (and difficult to find in the literature) we use K_{eq} and k_{diss} to calculate k_{prec}. The dissolution reaction constant k_{diss} is given by the Arrhenius equation

$$k_{diss} = Ae^{-\frac{E_a}{RT}} \tag{2.37}$$

where A is the Arrhenius pre-exponential factor, E_a the activation energy, R the universal gas constant and T the temperature in Kelvin [11] [12]. In the final model this equation is not used due to a simplification explained in section 3.3.

One of the many ways to express the equilibrium constant K_{eq} is given by:

$$log_{10} K_{eq} = A_1 + A_2 T + \frac{A_3}{T} + A_4 log_{10} T + \frac{A_5}{T^2} + A_6 T^2 \tag{2.38}$$

See table 2.1 for the values of A_1 up to and including A_6. Temperature T is in Kelvin.

Constant	Value
A_1	$3.55 \cdot 10^3$
A_2	1.21
A_3	$-1.33 \cdot 10^5$
A_4	$-1.41 \cdot 10^3$
A_5	$5.08 \cdot 10^6$
A_6	$-4.55 \cdot 10^{-4}$

Table 2.1: Equilibrium constants for K_{eq} [2].

At equilibrium the reaction term equals zero, then the equilibrium concentration $C_0(T)$ (dependent on temperature T (in Kelvin)) is given by:

$$\begin{aligned} \frac{\gamma_A \gamma_B C_0 \cdot C_B}{K_{eq}(T)} - 1 &= 0 \\ C_0(T) &= \frac{K_{eq}(T)}{\gamma_A \gamma_B C_B} \end{aligned} \tag{2.39}$$

At $t = 0$, the temperature T equals T_{high}, this gives the initial concentration of the porous medium (C_{pm}).

$$C_0(T_{high}) = C_{pm} = \frac{K_{eq}(T_{high})}{\gamma_A \gamma_B C_B} \tag{2.40}$$

This gives our new concentration equation in dimensionless form:

$$\frac{\partial C_d}{\partial t_d} = \frac{\mathcal{D}}{\phi} \frac{t_c}{d_c} \nabla^2 C_d - \frac{1}{\phi} \frac{t_c u_c}{d_c} \nabla \cdot (C_d \overrightarrow{u_d}) + A k_{diss} t_c C_d \tag{2.41}$$

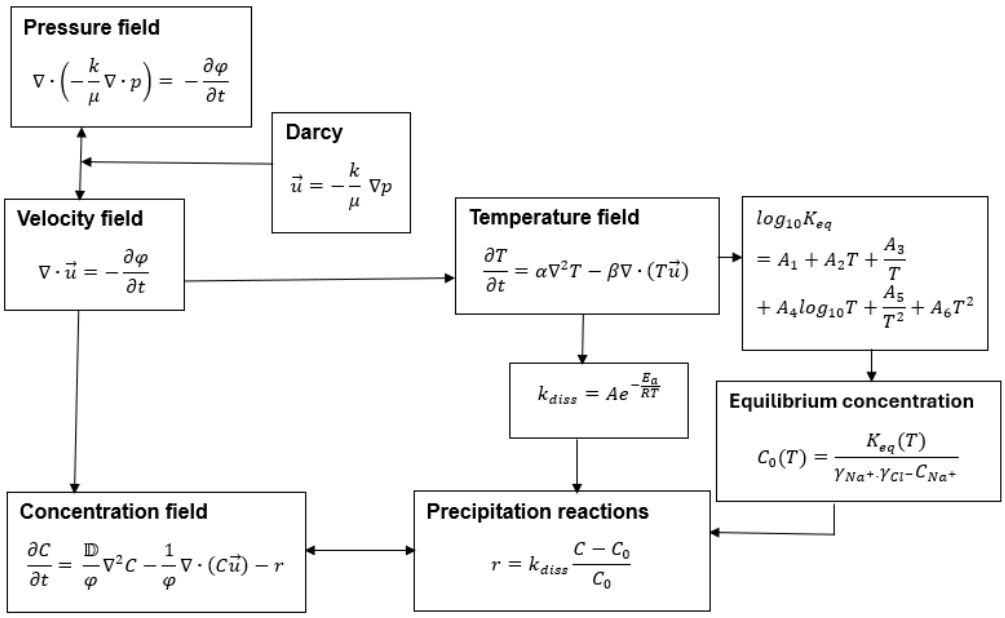

Figure 2.7: The schematic representation of the model derived thus far.

Since precipitation reactions are now implemented in the concentration model, the porosity ϕ and also the permeability k are not constant in time. Therefore the following equations have changed:

$$\nabla \cdot (-\frac{k}{\mu}\nabla p) = -\frac{\partial \phi}{\partial t} \tag{2.42}$$

Similar for the velocity

$$\nabla \cdot (\vec{u}) = -\frac{\partial \phi}{\partial t} \tag{2.43}$$

We assume that the relation between the porosity ϕ and the permeability k is given by [13]:

$$k = \frac{d^2}{180}\left(\frac{\phi^3}{(1-\phi)^2}\right) \tag{2.44}$$

with d the size of the gains.

In this model we assume that precipitation occurs when the concentration of species A (C) is higher than the equilibrium concentration $C_0(T)$. The surplus with respect to the equilibrium concentration will precipitate. When C is lower than C_0, there will be a deficit with respect to the equilibrium concentration and this will dissolve the solid salt. The amount of precipitation P is calculated by taking the difference between C and C_0 which is defined as

$$P = C - C_0 \tag{2.45}$$

2.8 Overview of the model

Figure 2.8 shows the schematic of the derived model. Now each arrow in this model will be explained:

1. The relation between the pressure and velocity equation given by the law of Darcy.
2. The influence of the velocity field on the temperature field given by the convection term.
3. The dissolution reaction constant k_{diss} is temperature dependent. The factor influences the precipitation reaction.
4. Similar to k_{diss} is the equilibrium constant K_{eq} dependent on temperature. The equilibrium concentration C_0 can be calculated with this equilibrium constant.
5. Similar to k_{diss}, the equilibrium concentration influences the precipitation reaction.
6. Similar to arrow 2, the velocity field influences the concentration field.
7. Arrow 7 combines the concentration equation and the precipitation reaction to yield a concentration field.
8. Arrow 8 defines when precipitation occurs, so for $C_0 < C$. Similar for dissolution. For further explanation, see section 3.3.
9. The amount of precipitation is calculated by taking the difference between the concentration and the equilibrium concentration.
10. Arrow 10 couples the amount of precipitation to the porosity ϕ.
11. Permeability k is calculated via the Kozeny-Carman relation using the porosity ϕ.
12. Arrow 12 represents the feedback from the change in porosity and permeability to the pressure and the velocity field.

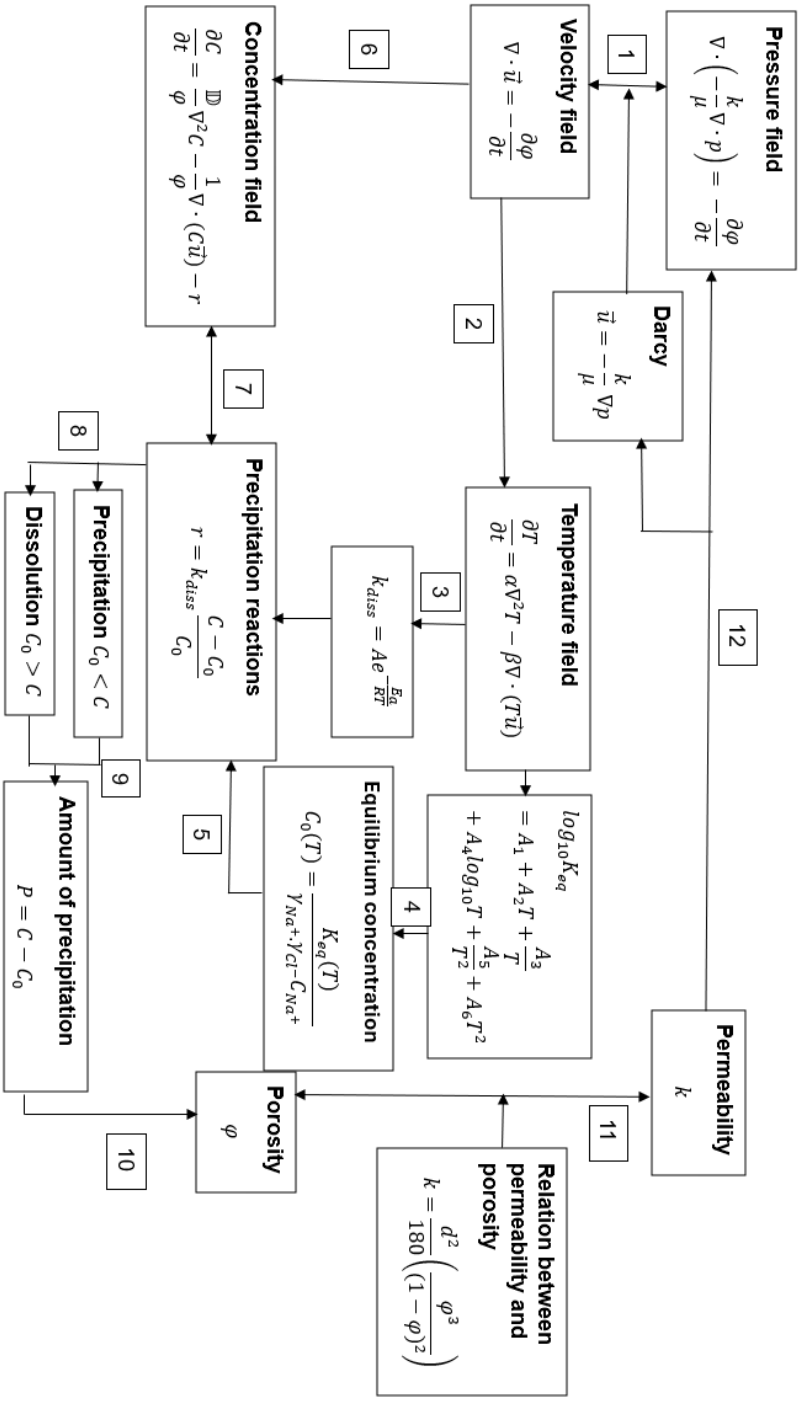

Figure 2.8: The schematic of the derived model, showing the connections between the variables.

Results

3.1 Pressure and velocity field

In this section, the pressure and velocity equations will be solved numerically and analytically. The analytical solution is possible due to the chosen equation and boundary conditions (see section 2.5). We verify the numerical approximation with this analytical solution of the pressure field.

3.1.1 Numerical approximation of the pressure and velocity field

For the numerical approximation in this model the 2D domain $[0, L] \times [0, H]$ has been divided in small rectangles of $\Delta x \times \Delta y$ with $\Delta x = \frac{L}{n_x}$ and $\Delta y = \frac{H}{n_y}$. Here n_x and n_y are the number of grid points in the x-direction and y-direction respectively. We choose n_x and n_y such that Δx and Δy are very small.

$p_{i,j}$ is the numerical approximation of pressure at location $[(i + \frac{1}{2})\Delta x, (j + \frac{1}{2})\Delta y]$ (Figure 3.1). Similarly for $\kappa_{i,j} := \frac{k}{\mu}_{i,j}$. Equation 2.15 will be approximated with the central difference method (see appendix A.3), because of its simplicity and it gives an accurate enough approximation of our flow. This numerical method will yield a linear matrix equation, that is solved by the python solver: numpy.linalg.solve(). When the pressure field is calculated, the velocities can be derived from the Darcy model (equation 2.1) by approximating the pressure gradient with the difference between two grid points. A staggered grid is used to connect the velocity field with the pressure field (see Figure 3.1). The numerical solution of the velocity field $\vec{u}$ is given in Figure 3.2.

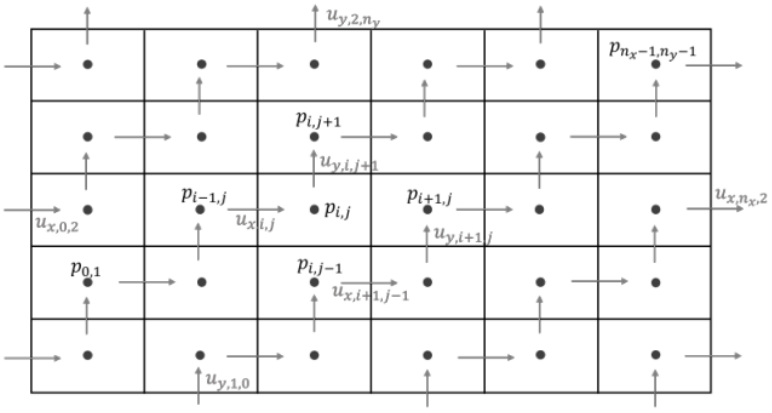

Figure 3.1: Discretization of scalar pressure p and vector velocity $\vec{u}$.

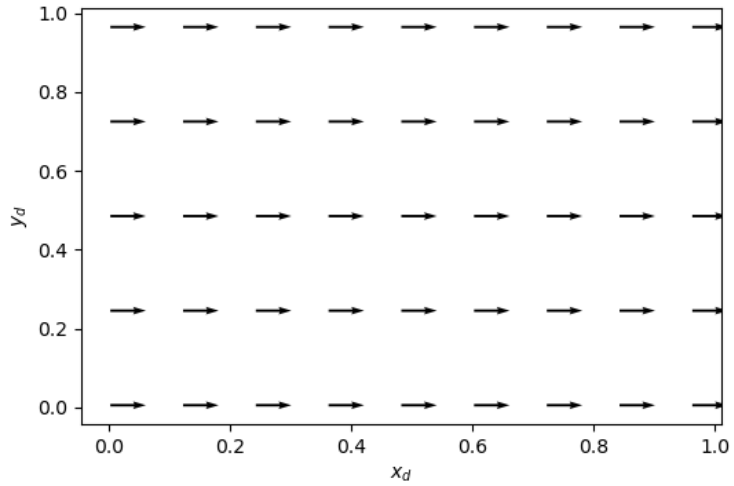

Figure 3.2: The numerical solution of the velocity field $\overrightarrow{u}$ with the arrows indicating the magnitude and direction of the Darcy velocity.

3.1.2 Analytical solution for the pressure field

Now we will solve equation 2.15 analytically. We start with assuming that $\frac{k}{\mu}$ is constant in space, as follows

$$\begin{cases} \nabla^2 p = 0 \\ \frac{\partial p}{\partial y}(x,0) = \frac{\partial p}{\partial y}(x,H) = 0 \\ \frac{\partial p}{\partial x}(0,y) = -\frac{u_0 \mu}{k} \\ \frac{\partial p}{\partial x}(L,y) = -\frac{u_0 \mu}{k} \end{cases} \tag{3.1}$$

Observe that $q(x,y) = -\frac{u_0 \mu}{k} x$ is a solution that satisfies the boundary conditions: $\frac{\partial p}{\partial x}(0,y) = \frac{\partial p}{\partial x}(L,y) = -\frac{u_0 \mu}{k}$.

Now define $r(x,y) := p(x,y) - q(x,y)$, as follows

$$\begin{cases} \nabla^2 r = \nabla^2 (p-q) = \nabla^2 p = 0 \\ \frac{\partial r}{\partial y}(x,0) = \frac{\partial r}{\partial y}(x,H) = 0 \\ \frac{\partial r}{\partial x}(0,y) = \frac{\partial p}{\partial x}(0,y) - \frac{\partial q}{\partial x}(0,y) = -\frac{u_0 \mu}{k} + \frac{u_0 \mu}{k} = 0 \\ \frac{\partial r}{\partial x}(L,y) = \frac{\partial p}{\partial x}(L,y) - \frac{\partial q}{\partial x}(L,y) = -\frac{u_0 \mu}{k} + \frac{u_0 \mu}{k} = 0 \end{cases} \tag{3.2}$$

To solve the following equations, we used the separation of variables method (see appendix A.6).

The dimensionless solution for the pressure field, as follows

$$p_d = -\frac{u_0 \mu d_c}{k p_c} x_d + \frac{p_0}{p_c} \tag{3.3}$$

3.1.3 Results of the pressure field

The numerical and analytical solution of the pressure field p is given in Figure 3.3 and the relative difference between them is given in Figure 3.4.

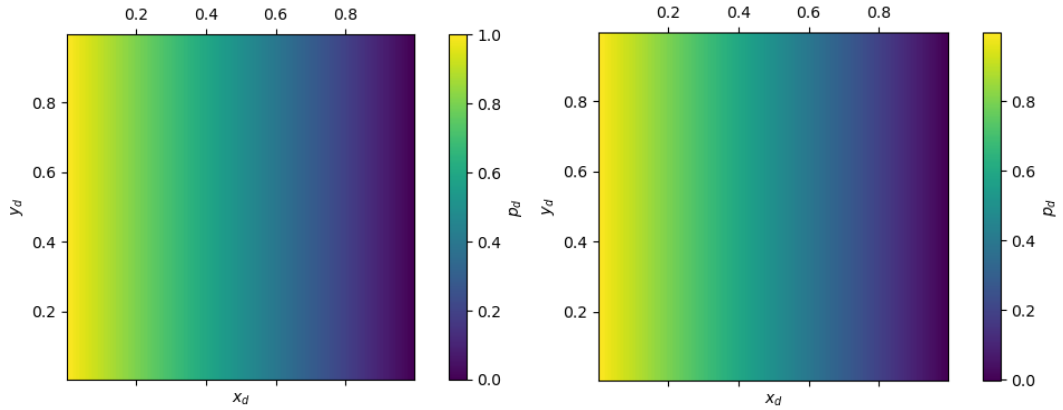

(a) The numerical solution of the pressure field p expressed in the dimensionless pressure p_d.

(b) Analytical solution of the pressure field p expressed in the dimensionless p_d.

Figure 3.3: The numerical and analytical solution for equation 2.16 on the dimensionless domain (x_d, y_d).

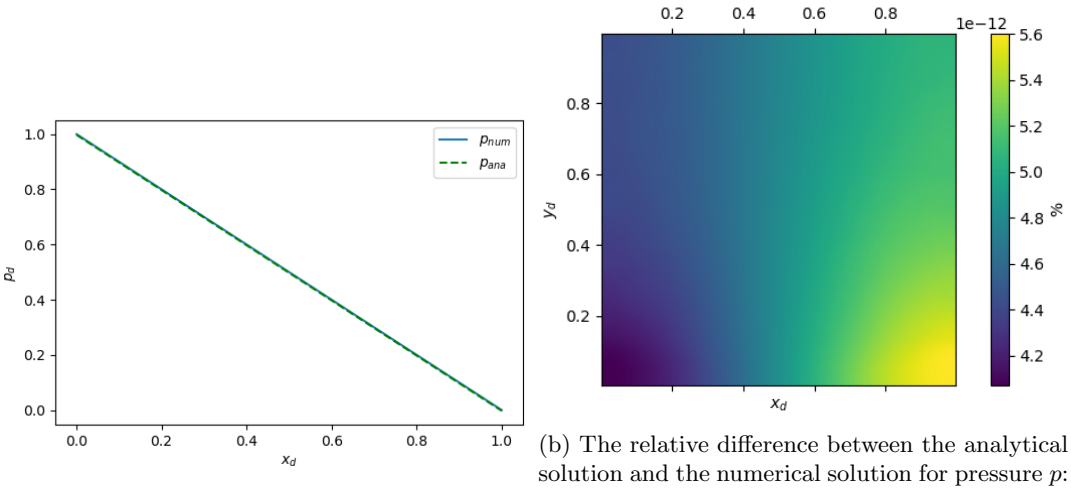

(a) The numerical and analytical solution for pressure p plotted in the x-direction. There is little or no visible difference between the two solutions.

(b) The relative difference between the analytical solution and the numerical solution for pressure p: $(p_{num} - p_{ana})/max(p_{num}) \cdot 100\%$. The difference between the two solutions is at most $5 \cdot 10^{-12}\%$, so a minimal difference.

Figure 3.4: The analytical and numerical solution for equation 2.16 and the relative difference on the dimensionless domain (x_d, y_d).

To find the accuracy of a numerical method, the numerical solutions are compared with the analytical solution. In this case, the numerical and analytical solution of the pressure equation were almost identical and therefore the numerical approximation is very accurate.

3.2 Temperature Distribution

In this section, the temperature equation will be solved numerically and analytically.

3.2.1 Numerical approximation of the temperature distribution

$T_{i,j}$ is the numerical approximation of pressure at location $[(i+\frac{1}{2})\Delta x, (j+\frac{1}{2})\Delta y]$. Equation 2.22 will be approximated with several numerical methods (see appendix A.4) Similar to the pressure, equation 2.22 will be approximated by the central difference and for time derivative terms forward Euler will be used. The stability of the forward Euler is checked in section A.8. The numerical solution for equation 2.24 is given in Figure 3.5 and 3.6.

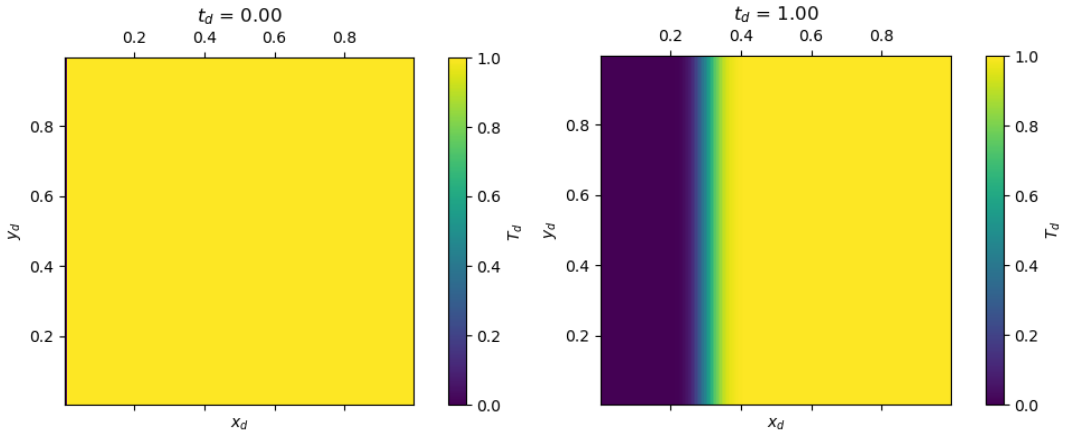

(a) Temperature distribution T at $t_d = 0$ expressed in the dimensionless temperature T_d.

(b) Temperature distribution T at $t_d = 1$ expressed in the dimensionless temperature T_d.

Figure 3.5: The numerical solution for equation 2.24 on the dimensionless domain (x_d, y_d).

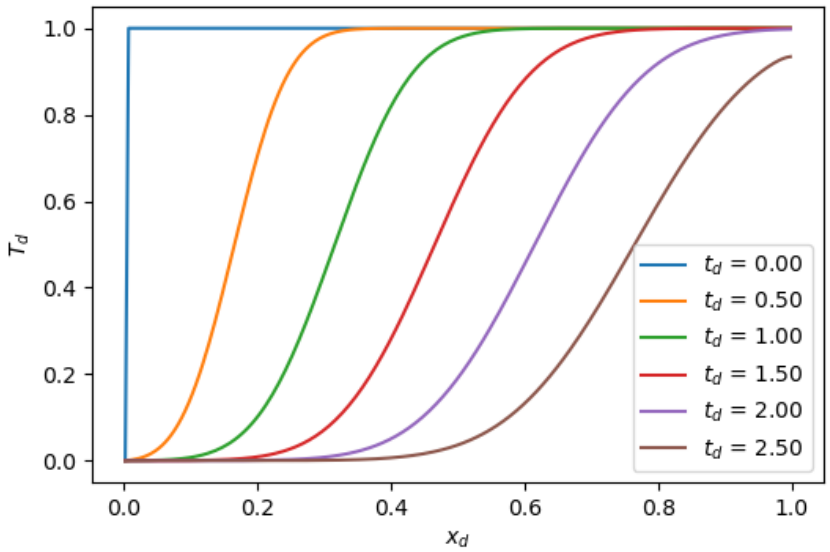

Figure 3.6: The numerical solution for the dimensionless temperature distribution T_d plotted in the x-direction.

3.2.2 Analytical solution for the temperature distribution

Now we will solve equation 2.22 with boundary conditions 2.23 analytically. We start with assuming that the Darcy velocity $\overrightarrow{u}$ is constant in space and substitute $\gamma = \beta\overrightarrow{u}$, as follows

$$\begin{cases} \frac{\partial T}{\partial t} = \alpha\nabla^2 T - \gamma\nabla \cdot T \\ T(0,y,t) = T_{low} \\ \frac{\partial T}{\partial x}(L,y,t) = 0 \\ \frac{\partial T}{\partial y}(x,0,t) = 0 \\ \frac{\partial T}{\partial y}(x,H,t) = 0 \\ T(x>0,y,0) = T_{high} \end{cases} \tag{3.4}$$

Now assume that $\alpha \neq 0$, $\gamma \neq 0$ and we neglect the y-component of the heat equation. We get a 1D heat equation:

$$\frac{\partial T}{\partial t} = \alpha\frac{\partial^2 T}{\partial x^2} - \gamma\frac{\partial T}{\partial x} \tag{3.5}$$

With $\gamma = \beta\overrightarrow{u}$. For a solution of this heat equation try:

$$T(x,t) = e^{-\frac{\gamma^2}{4\alpha}t}e^{\frac{\gamma}{2\alpha}t}v(x,t) := Av(x,t)[14] \tag{3.6}$$

Substituting 3.6 into equation 3.5, as follows

$$\begin{aligned} -\frac{\gamma^2}{4\alpha}Av + A\frac{\partial v}{\partial t} &= \alpha\left(\frac{\gamma^2}{4\alpha^2}Av + 2\frac{\gamma}{2\alpha}A\frac{\partial v}{\partial x} + A\frac{\partial^2 v}{\partial x^2}\right) - \gamma\left(\frac{\gamma}{2\alpha}Av + A\frac{\partial v}{\partial x}\right) \\ A\frac{\partial v}{\partial t} &= \left(2\frac{\gamma^2}{4\alpha} - \frac{\gamma^2}{2\alpha}\right)Av + (\gamma-\gamma)A\frac{\partial v}{\partial x} + \alpha A\frac{\partial^2 v}{\partial x^2} \\ \frac{\partial v}{\partial t} &= \alpha\frac{\partial^2 v}{\partial x^2} \end{aligned} \tag{3.7}$$

So now we get our new problem:

$$\begin{cases} \frac{\partial v}{\partial t} = \alpha\frac{\partial^2 v}{\partial x^2} \\ v(0,t) = 0 \\ \frac{\gamma}{2\alpha}v(L,t) + \frac{\partial v}{\partial x}(L,t) = 0 \\ e^{\frac{\gamma}{2\alpha}x}v(x>0,0) = \Delta T \end{cases} \tag{3.8}$$

Here we use separation of variables (see appendix A.7). The dimensionless solution, as follows

$$T_d(x,t) = \sum_{n=1}^{\infty}\frac{c_n}{\Delta T}e^{-(\frac{\gamma^2}{4\alpha}+\lambda_n\alpha)t_c t_d}e^{\frac{\gamma}{2\alpha}d_c x_d}sin(\sqrt{\lambda_n}d_c x_d) \tag{3.9}$$

With:

$$c_n = \frac{\int_0^1 \Delta T e^{-\frac{\gamma d_c}{2\alpha}x_d}sin(\sqrt{\lambda_n}d_c x_d)dx_d}{\int_0^1 sin^2(\sqrt{\lambda_n}d_c x_d)dx_d} \tag{3.10}$$

3.2.3 Results of the temperature distribution

This analytical solution is given in figure 3.7.

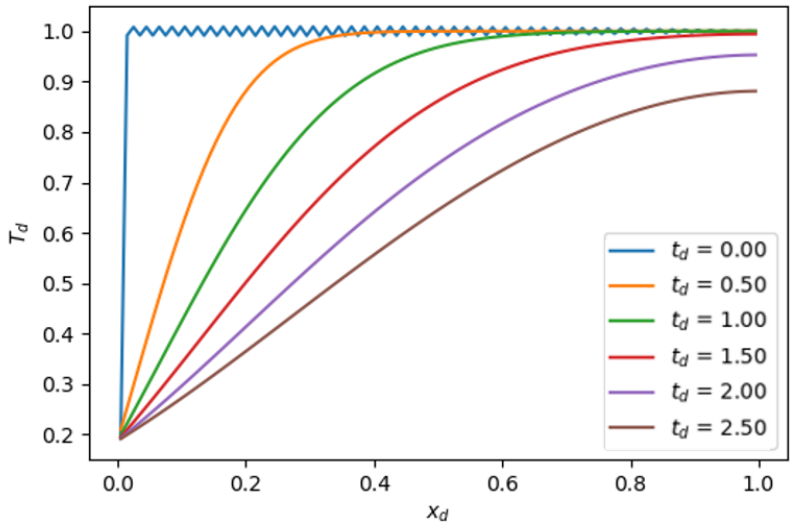

Figure 3.7: The analytical solution for equation 2.24 with neglection of the y-component. The temperature distribution T is expressed in the dimensionless temperature T_d.

The analytical problem could not be solved purely through analytical methods, because the eigenvalues and therefore also the eigenfunctions are too complicated to solve by hand. We used numerical methods for the derivation of the eigenvalues and therefore some errors from the numerical computation influenced the results of the analytical solution. Therefore the accuracy of the numerical model for the temperature distribution could not be determined with certainty. The numerical methods used in the simulation are stable for $\Delta t_d \leqslant 0.03$ (see A.8).

The aquifer is defined as completely cooled if the temperature on the right side of the aquifer is less than 40 $^\circ C$. For a constant $\kappa = \frac{k}{\mu}$ in time and space, the aquifer is fully cooled after $1.83 \cdot 10^8$ s ($t_d = 3.39$), which is 5.803 years.

3.3 Concentration field

3.3.1 Numerical approximation of the concentration field

For the numerical approximation of the concentration equation some considerable simplifications have been applied.

1. Only two species A and B are involved in the precipitation reaction. In this model we choose Na^+ as species B and Cl^- as species A. Both these minerals have the highest concentration of all the minerals in water. The precipitation reaction will form solid salt ($NaCl$):

$$NaCl \leftrightarrow Na^+ + Cl^- \tag{3.11}$$

2. The concentration of Na^+ is much larger than the concentration of Cl^- [2]. Therefore the production of $NaCl$ only depends on the concentration of Cl^-. Furthermore, the concentration of Na^+ remains constant in time and space.

3. The change in porosity ϕ and permeability k due to precipitation has no influence on the pressure, velocity and temperature distribution (A). This simplification is done because the pressure/velocity equation then gets an extra time-dependent term, which complicates the solution considerably. This simplification is allowed when the change in porosity ϕ and permeability k is negligibly small.

4. Precipitation occurs when the concentration of Cl^- (C) is higher than the equilibrium concentration $C_0(T)$. The surplus with respect to the equilibrium concentration will precipitate. When C is lower than C_0, there will be a deficit with respect to the equilibrium concentration and this will dissolve the solid salt (B).

5. At each time step Δt, the concentration C will approach the equilibrium concentration C_0 through the concentration field equation. Then we calculate the amount of precipitation P by taking the difference between C and C_0 (arrow C) which is defined as

$$P = C - C_0 \tag{3.12}$$

   So for $P > 0$ we have precipitation of Cl^-, which will form solid salt and for $P < 0$ we have dissolution of Cl^-. After each time step, we set the concentration C equal to C_0 and begin the next time step (arrow D). This simplification is only allowed when the timescale of the precipitation reactions are almost similar to the timescale of the convection/diffusion reactions. The first Dahmköhler number (Da_I) quantifies the ratio of the reaction timescale to the transport timescale and is defined in this model as [2]

$$Da_I = \frac{Ak_{diss}d_c}{C_0 u_c} \simeq 1 \tag{3.13}$$

The schematic of the simplified model described is shown in Figure 3.8.

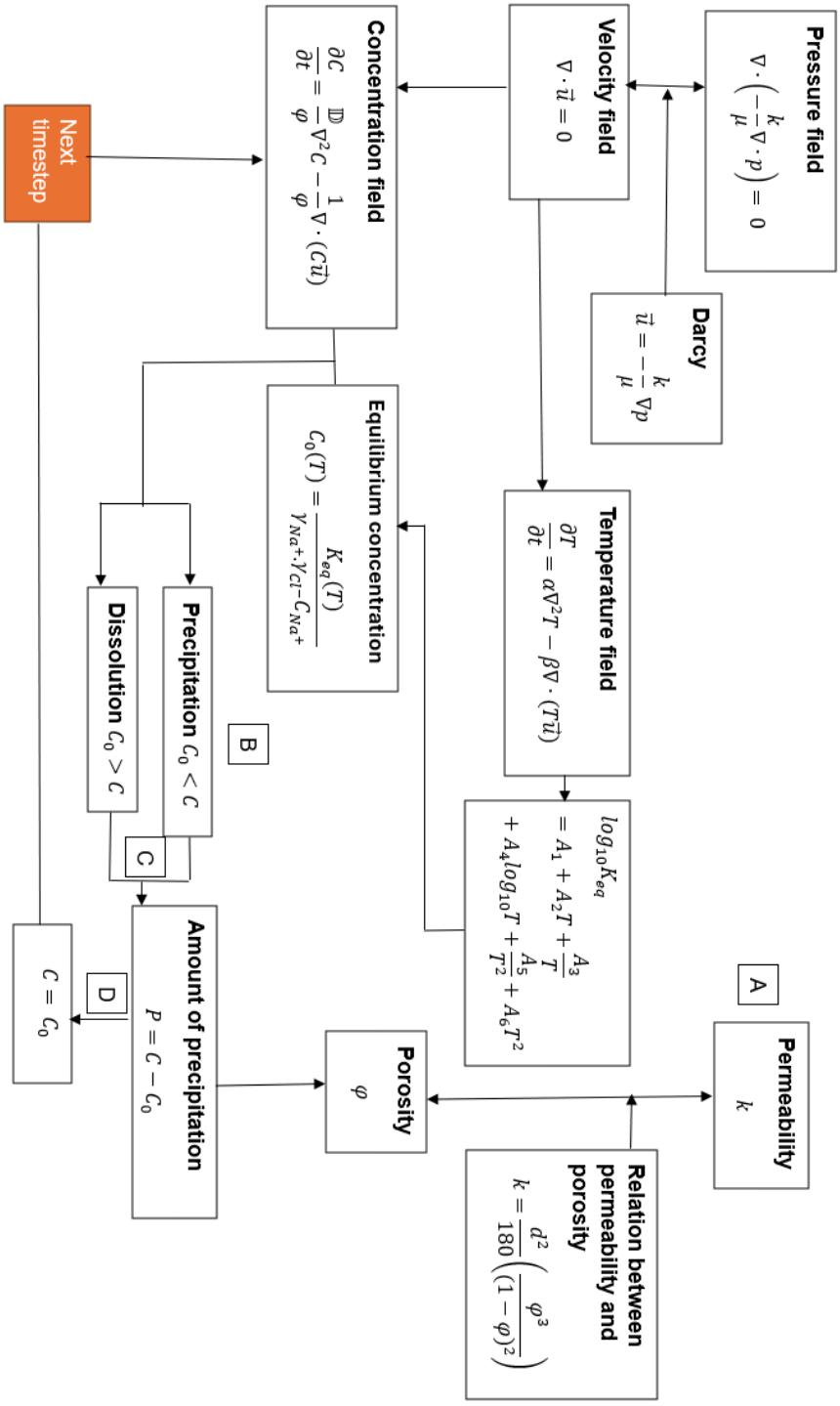

Figure 3.8: The schematic of the simplified model, showing the connections between the variables.

3.3.2 Results of the concentration field

$$\frac{\partial C}{\partial t} = \frac{\mathcal{D}}{\phi}\nabla^2 C - \frac{1}{\phi}\nabla \cdot (C\vec{u}) \tag{3.14}$$

$C_{i,j}$ is the numerical approximation of pressure at location $[(i+\frac{1}{2})\Delta x, (j+\frac{1}{2})\Delta y]$. Equation 3.14 will be approximated with several numerical methods (see appendix A.5) Similar to the temperature, equation 3.14 will be approximated by the central difference and for time derivative terms forward Euler will be used. The stability of the forward Euler is checked in section A.8. This concentration field C is shown in Figure 3.9.

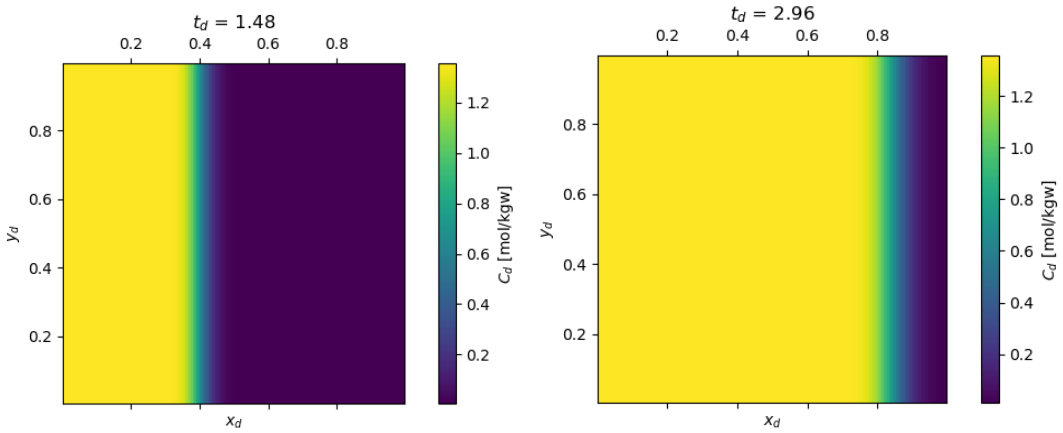

(a) $t_d = 1.48$ (b) $t_d = 2.96$

Figure 3.9: The concentration field C at different t_d expressed in the dimensionless concentration C_d.

From the model we get an amount of precipitation in mol per kg water. This is equal to the concentration of solid salt ($NaCl$) due to the 1:1-reaction. Via the molar mass of $NaCl$ (M_{NaCl} = 0.05844 kg/mol), we can calculate the amount of kg $NaCl$ per kg water. Via the density of $NaCl$ ($\rho_{NaCl} = 2.163 \cdot 10^3\ kg/m^3$), we can calculate the total volume that is occupied by the solid salt taking into account the initial porosity ϕ_0 and the volume of a cell V_{cell} as follows

$$\phi = \phi_0 - \frac{P}{V_{cell}} \tag{3.15}$$

See Figure 3.10 for the amount of precipitation P expressed in mol $NaCl$ and in m^3 $NaCl$ per kg water. In Figure 3.11 we calculated the porosity via equation 3.15 and the permeability via equation 2.44.

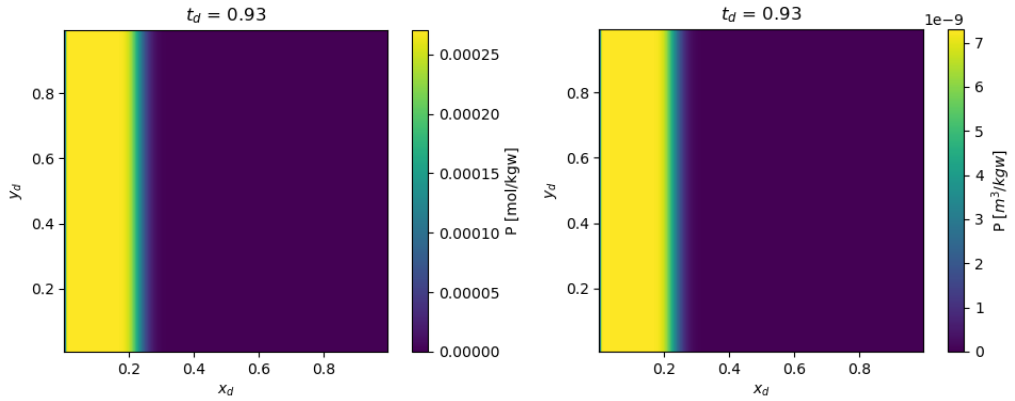

(a) The amount of precipitation P expressed in mol $NaCl$ per kg water.

(b) The amount of precipitation P expressed in m^3 $NaCl$ per kg water.

Figure 3.10: The amount of precipitation P for normal C_0 expressed in mol $NaCl$ and in m^3 $NaCl$ per kg water.

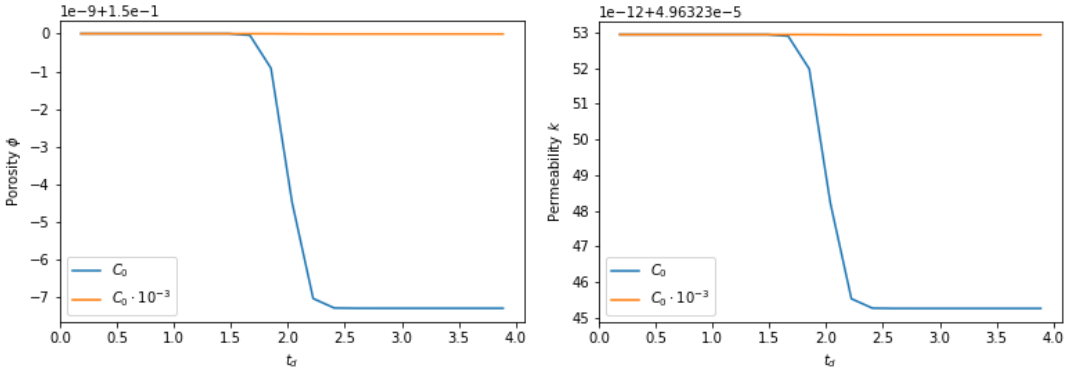

(a) Porosity ϕ for different values of C_0.

(b) Permeability k for different values of C_0.

Figure 3.11: The porosity ϕ and the permeability k at halfway the domain for different values of C_0.

Since the amount of precipitation was very small, the change in porosity ϕ is in the order of 10^{-9} and the change in permeability in the order of 10^{-12} for a normal C_0. For $C_0 \cdot 10^{-3}$, the change in ϕ and k is even smaller. If we increase the initial concentration of Cl^-, we get a larger decrease in porosity, but then the simplifications in the numerical approximation are not justified.

Conclusion

As outlined in the introduction, this study aims to investigate the sustainability of geothermal energy in an aquifer. We divided this research goal into two subquestions:

How long does it take for the geothermal aquifer to cool?

How long does it take for the geothermal aquifer to clog due to precipitation reactions?

To address these questions, we performed numerical simulations based on pressure equations, heat transport equations and chemical reaction kinetics.

- The numerical and analytical solution of the pressure equation were almost identical and therefore the numerical approximation for the pressure equation is very accurate.
- The introduction of colder water alters the composition and temperature of the water in the aquifer. These changes influence chemical equilibria, potentially leading to the dissolution or precipitation of certain minerals.
- The analytical problem could not be solved purely through analytical methods. We used numerical methods for the derivation of the eigenvalues and therefore some errors from the numerical computation influenced the results of the analytical solution. Therefore the accuracy of the numerical model for the temperature distribution could not be determined with certainty. The numerical methods used in the simulation are stable for $\Delta t_d \leqslant 0.03$.
- The aquifer is defined as completely cooled if the temperature on the right side of the aquifer is less than 40 $^\circ C$. For a constant $\kappa = \frac{k}{\mu}$ in time and space, the aquifer is fully cooled after $1.83 \cdot 10^8$ s ($t_d = 3.39$), which is 5.803 years. The is not realistic because we neglected the heat supply from the earth core and chose simplified boundary conditions (see chapter 5). Therefore (depending on the amount of heat supply and the chosen boundary conditions) the aquifer will take longer to fully cool. However, in this model, the use of geothermal energy is not sustainable in terms of temperature.
- Since the amount of precipitation was very small, the change in porosity ϕ is in the order of 10^{-9} and therefore in this model porosity and permeability will not play a significant role in sustainability of the geothermal system.
- The simplifications in the numerical approximation were justified, since ϕ and k were negligibly small.

Discussion

In this project, we examined the sustainability of a geometric aquifer and the results above provided significant insights. However, several results raised important questions about model extensions and the aquifers' long-term viability.

- According to the result above, the aquifer is cooled after almost 6 years. This is not entirely accurate, because the boundary conditions that were selected were not fully chosen to reflect the complexities of the system. We also didn't properly consider the heat coming from Earth's core. As a result, the cooling time of the aquifer was significantly faster than anticipated. For a possible model extension, we can introduce a heat source Q and use the boundary conditions explained in [15].
- This study did not investigate the microscopic-level concentration distributions, which could play a critical role in understanding the chemical interactions within the aquifer.
- In this model we neglected the influence of change in porosity ϕ and permeability k due to precipitation on the pressure, velocity and temperature distribution. In this model this was allowed, because the change in porosity ϕ and permeability k were negligibly small. In possible model extension, this might not be the case (different choice of mineral).
- A possible report extension can answer the question:

  How can we prevent mineral precipitation in a geothermal aquifer to keep it sustainable?

  Examples of solutions are the use of heat exchangers or chemical inhibitors.
- In our model, we assume that the change in K_{eq} is only influenced by change in temperature. We assume that the effects of change in pH are negligible. The effects of the change in pH can be added to a possible model extension.

Appendix

A.1 Divergence theorem

The Divergence Theorem (also known as Gauss's Theorem) is a fundamental result in vector calculus. It relates the flow of a vector field through a closed surface to the divergence of the field within the volume enclosed by that surface. Mathematically, it is expressed as:

$$\int_V (\nabla \cdot \mathbf{F})\, dV = \oint_{\partial V} \mathbf{F} \cdot \mathbf{n}\, dS \tag{A.1}$$

where $\mathbf{F}$ is a vector field, $\nabla \cdot \mathbf{F}$ is the divergence of $\mathbf{F}$, ∂V the closed surface bounding the volume V, $\mathbf{n}$ is the outward unit vector to the surface ∂V, dV and dS are respectively volume and surface elements.

In essence, the theorem states that the total outward flux of a field through a closed surface is equal to the integral of the divergence of the field over the volume enclosed by the surface.

A.2 Derivation heat equation

$$\frac{\partial T_w}{\partial t} = \frac{a_w}{\phi}\nabla^2 T_w - \frac{1}{\phi}\nabla \cdot (T_w \overrightarrow{u}) + \frac{hA}{c_w \rho_w \phi V}(T_{pm} - T_w) \tag{A.2}$$

$$\frac{\partial T_{pm}}{\partial t} = \frac{a_{pm}}{1-\phi}\nabla^2 T_{pm} - \frac{hA}{c_{pm}\rho_{pm}(1-\phi)V}(T_{pm} - T_w) \tag{A.3}$$

With $T_w \approx T_{pm} := T$ we get:

$$(c_w \rho_w \phi + c_{pm}\rho_{pm}(1-\phi))\frac{\partial T}{\partial t} = (c_w \rho_w a_w + c_{pm}\rho_{pm} a_{pm})\nabla^2 T - c_w \rho_w \nabla \cdot (T\overrightarrow{u}) \tag{A.4}$$

A.3 Numerical approximation pressure field

$$\nabla p \approx \frac{p_{i+\frac{1}{2},j} - p_{i-\frac{1}{2},j}}{\Delta x}\hat{x} + \frac{p_{i,j+\frac{1}{2}} - p_{i,j-\frac{1}{2}}}{\Delta y}\hat{y} \tag{A.5}$$

For $\kappa_{i+\frac{1}{2},j}$ we use the mean of the 2 boundary points.

$$\kappa_{i+\frac{1}{2},j} := \frac{2}{\frac{1}{\kappa_{i,j}} + \frac{1}{\kappa_{i+1,j}}} \tag{A.6}$$

$$\nabla \cdot (-\kappa \nabla p) \approx \frac{-\kappa_{i+\frac{1}{2},j}\frac{p_{i+1,j}-p_{i,j}}{\Delta x} + \kappa_{i-\frac{1}{2},j}\frac{p_{i,j}-p_{i-1,j}}{\Delta x}}{\Delta x} + \frac{-\kappa_{i,j+\frac{1}{2}}\frac{p_{i,j+1}-p_{i,j}}{\Delta y} + \kappa_{i,j-\frac{1}{2}}\frac{p_{i,j}-p_{i,j-1}}{\Delta y}}{\Delta y} \tag{A.7}$$

$$= \frac{-\kappa_{i+\frac{1}{2},j}p_{i+1,j} + (\kappa_{i+\frac{1}{2},j} + \kappa_{i-\frac{1}{2},j})p_{i,j} - \kappa_{i-\frac{1}{2},j}p_{i-1,j}}{\Delta x^2} + \frac{-\kappa_{i,j+\frac{1}{2}}p_{i,j+1} + (\kappa_{i,j+\frac{1}{2}} + \kappa_{i,j-\frac{1}{2}})p_{i,j} - \kappa_{i,j-\frac{1}{2}}p_{i,j-1}}{\Delta y^2} \tag{A.8}$$

$$\begin{cases} \frac{\partial p}{\partial x}(0,y) \approx \frac{p_{0,j}-p_{-1,j}}{\Delta x} = -\frac{u_0}{\kappa_{-\frac{1}{2},j}} \\ \frac{\partial p}{\partial x}(L,y) \approx \frac{p_{n_x,j}-p_{n_x-1,j}}{\Delta x} = -\frac{u_0}{\kappa_{n_x-\frac{1}{2},j}} \\ \frac{\partial p}{\partial y}(x,0) \approx \frac{p_{i,0}-p_{i,-1}}{\Delta y} = 0 \\ \frac{\partial p}{\partial y}(x,H) \approx \frac{p_{i,n_y}-p_{i,n_y-1}}{\Delta y} = 0 \end{cases} \tag{A.9}$$

For $0 < i < n_x - 1$ and $0 < j < n_y - 1$, we have:

$$\frac{-\kappa_{i+\frac{1}{2},j}p_{i+1,j} + (\kappa_{i+\frac{1}{2},j} + \kappa_{i-\frac{1}{2},j})p_{i,j} - \kappa_{i-\frac{1}{2},j}p_{i-1,j}}{\Delta x^2} + \frac{-\kappa_{i,j+\frac{1}{2}}p_{i,j+1} + (\kappa_{i,j+\frac{1}{2}} + \kappa_{i,j-\frac{1}{2}})p_{i,j} - \kappa_{i,j-\frac{1}{2}}p_{i,j-1}}{\Delta y^2} = 0 \tag{A.10}$$

Now for the boundary conditions:
For $i = 0$ and $j = 0$, we have:

$$\frac{-\kappa_{i+\frac{1}{2},j}p_{i+1,j} + \kappa_{i+\frac{1}{2},j}p_{i,j}}{\Delta x^2} + \frac{-\kappa_{i,j+\frac{1}{2}}p_{i,j+1} + \kappa_{i,j+\frac{1}{2}}p_{i,j}}{\Delta y^2} = \frac{u_0}{\Delta x} \tag{A.11}$$

For $i = 0$ and $0 < j < n_y - 1$, we have:

$$\frac{-\kappa_{i+\frac{1}{2},j}p_{i+1,j} + \kappa_{i+\frac{1}{2},j}p_{i,j}}{\Delta x^2} + \frac{-\kappa_{i,j+\frac{1}{2}}p_{i,j+1} + (\kappa_{i,j+\frac{1}{2}} + \kappa_{i,j-\frac{1}{2}})p_{i,j} - \kappa_{i,j-\frac{1}{2}}p_{i,j-1}}{\Delta y^2} = \frac{u_0}{\Delta x} \tag{A.12}$$

For $0 < i < n_x - 1$ and $j = n_y - 1$, we have:

$$\frac{-\kappa_{i+\frac{1}{2},j}p_{i+1,j} + (\kappa_{i+\frac{1}{2},j} + \kappa_{i-\frac{1}{2},j})p_{i,j} - \kappa_{i-\frac{1}{2},j}p_{i-1,j}}{\Delta x^2} + \frac{-\kappa_{i,j-\frac{1}{2}}p_{i,j} + \kappa_{i,j-\frac{1}{2}}p_{i,j-1}}{\Delta y^2} = 0 \tag{A.13}$$

For $i = n_x - 1$ and $j = n_y - 1$, we have:

$$\frac{-\kappa_{i-\frac{1}{2},j}p_{i,j} + \kappa_{i-\frac{1}{2},j}p_{i-1,j}}{\Delta x^2} + \frac{-\kappa_{i,j-\frac{1}{2}}p_{i,j} + \kappa_{i,j-\frac{1}{2}}p_{i,j-1}}{\Delta y^2} = -\frac{u_0}{\Delta x} \tag{A.14}$$

A.4 Numerical approximation temperature distribution

$$\nabla^2 T = \frac{T^k_{i+1,j} - 2T^k_{i,j} + T^k_{i-1,j}}{\Delta x^2} + \frac{T^k_{i,j+1} - 2T^k_{i,j} + T^k_{i,j-1}}{\Delta y^2} \tag{A.15}$$

$$\nabla \cdot (T\overrightarrow{u}) = -\frac{u_{x,i+1,j}T^k_{i,j} - u_{x,i,j}T^k_{i-1,j}}{\Delta x} - \frac{u_{y,i,j+1}T^k_{i,j} - u_{y,i,j}T^k_{i,j-1}}{\Delta y} \tag{A.16}$$

$$\frac{\partial T}{\partial t} \approx \frac{T^{k+1}_{i,j} - T^k_{i,j}}{\Delta t} \tag{A.17}$$

Substituting A.15, A.16 and A.17 in 2.22:

$$\begin{aligned} T^{k+1}_{i,j} = T^k_{i,j} &+ \Delta t\alpha\left(\frac{T^k_{i+1,j} - 2T^k_{i,j} + T^k_{i-1,j}}{\Delta x^2} + \frac{T^k_{i,j+1} - 2T^k_{i,j} + T^k_{i,j-1}}{\Delta y^2}\right) \\ &+ \Delta t\beta\left(-\frac{u_{x,i+1,j}T^k_{i,j} - u_{x,i,j}T^k_{i-1,j}}{\Delta x} - \frac{u_{y,i,j+1}T^k_{i,j} - u_{y,i,j}T^k_{i,j-1}}{\Delta y}\right) \end{aligned} \tag{A.18}$$

$$\begin{cases} T(0,y,t) \approx T^k_{0,j} = T_{low} \\ \frac{\partial T}{\partial x}(L,y,t) \approx \frac{T^k_{n_x,j} - T^k_{n_x-1,j}}{\Delta x} = 0 \\ \frac{\partial T}{\partial y}(x,0,t) \approx \frac{T^k_{i,0} - T^k_{i,-1}}{\Delta y} = 0 \\ \frac{\partial T}{\partial y}(x,H,t) \approx \frac{T^k_{i,n_y} - T^k_{i,n_y-1}}{\Delta y} = 0 \\ T(x,y,0) \approx T^0_{i,j} = \begin{cases} T_{low}, i = 0 \\ T_{high}, i \neq 0 \end{cases} \end{cases} \tag{A.19}$$

For $0 < i < n_x - 1$ and $0 < j < n_y - 1$, we have equation A.18.

Now for the boundary conditions: For $i = n_x - 1$ and $0 < j < n_y - 1$, we have:

$$\begin{aligned} T^{k+1}_{n_x-1,j} = T^k_{n_x-1,j} + \Delta t\alpha\left(\frac{T^k_{n_x-1,j} + T^k_{n_x-2,j}}{\Delta x^2} + \frac{T^k_{n_x-1,j+1} - 2T^k_{n_x-1,j} + T^k_{n_x-1,j-1}}{\Delta y^2}\right) \\ +\Delta t\beta\left(-\frac{u_{x,n_x,j}T^k_{n_x-1,j} - u_{x,n_x-1,j}T^k_{n_x-2,j}}{\Delta x} - \frac{u_{y,n_x-1,j+1}T^k_{n_x-1,j} - u_{y,n_x-1,j}T^k_{n_x-1,j-1}}{\Delta y}\right) \end{aligned} \tag{A.20}$$

For $0 < i < n_x - 1$ and $j = 0$, we have:

$$\begin{aligned} T^{k+1}_{i,0} = T^k_{i,0} + \Delta t\alpha\left(\frac{T^k_{i+1,0} - 2T^k_{i,0} + T^k_{i-1,0}}{\Delta x^2} + \frac{T^k_{i,1} - T^k_{i,0}}{\Delta y^2}\right) \\ +\Delta t\beta\left(-\frac{u_{x,i+1,0}T^k_{i,0} - u_{x,i,0}T^k_{i-1,0}}{\Delta x} - \frac{(u_{y,i,1} - u_{y,i,0})T^k_{i,0}}{\Delta y}\right) \end{aligned} \tag{A.21}$$

For $= n_x - 1$ and $j = 0$

$$\begin{aligned} T^{k+1}_{n_x-1,0} = T^k_{n_x-1,0} + \Delta t\alpha\left(\frac{T^k_{n_x-1,0} - T^k_{n_x-2,0}}{\Delta x^2} + \frac{T^k_{n_x-1,1} - T^k_{n_x-1,0}}{\Delta y^2}\right) \\ +\Delta t\beta\left(-\frac{u_{x,n_x-1,0}T^k_{n_x-1,0} - u_{x,n_x-1,0}T^k_{n_x-2,0}}{\Delta x} - \frac{(u_{y,n_x-1,1} - u_{y,n_x-1,0})T^k_{n_x-1,0}}{\Delta y}\right) \end{aligned} \tag{A.22}$$

A.5 Numerical approximation concentration field

For the numerical approximation of equation 3.14, we use the same numerical methods as in the numerical approximation for pressure and temperature, as follows

$$\nabla^2 C = \frac{C^k_{i+1,j} - 2C^k_{i,j} + C^k_{i-1,j}}{\Delta x^2} + \frac{C^k_{i,j+1} - 2C^k_{i,j} + C^k_{i,j-1}}{\Delta y^2} \tag{A.23}$$

$$\nabla \cdot (C\overrightarrow{u}) = -\frac{u_{x,i+1,j}C^k_{i,j} - u_{x,i,j}C^k_{i-1,j}}{\Delta x} - \frac{u_{y,i,j+1}C^k_{i,j} - u_{y,i,j}C^k_{i,j-1}}{\Delta y} \tag{A.24}$$

$$\frac{\partial C}{\partial t} \approx \frac{C^{k+1}_{i,j} - C^k_{i,j}}{\Delta t} \tag{A.25}$$

We get:

$$\begin{aligned} C^{k+1}_{i,j} = C^k_{i,j} + \Delta t\frac{\mathcal{D}}{\phi}\left(\frac{C^k_{i+1,j} - 2C^k_{i,j} + C^k_{i-1,j}}{\Delta x^2} + \frac{C^k_{i,j+1} - 2C^k_{i,j} + C^k_{i,j-1}}{\Delta y^2}\right) \\ +\Delta t\frac{1}{\phi}\left(\frac{u_{x,i+1,j}C^k_{i,j} - u_{x,i,j}C^k_{i-1,j}}{\Delta x} + \frac{u_{y,i,j+1}C^k_{i,j} - u_{y,i,j}C^k_{i,j-1}}{\Delta y}\right) \end{aligned} \tag{A.26}$$

With boundary conditions:

$$\begin{cases} C(0,y,t) \approx C^k_{0,j} = C_{Cl^-} \\ \frac{\partial C}{\partial x}(L,y,t) \approx \frac{C^k_{nx,j} - C^k_{nx-1,j}}{\Delta x} = 0 \\ \frac{\partial C}{\partial y}(x,0,t) \approx \frac{C^k_{i,0} - C^k_{i,-1}}{\Delta y} = 0 \\ \frac{\partial C}{\partial y}(x,H,t) \approx \frac{C^k_{i,n_y} - C^k_{i,n_y-1}}{\Delta y} = 0 \\ C(x,y,0) \approx C^0_{i,j} = \begin{cases} C_{Cl^-}, i = 0 \\ C_{pm}, i \neq 0 \end{cases} \end{cases} \tag{A.27}$$

For $0 < i < n_x - 1$ and $0 < j < n_y - 1$, we have equation A.26.
Now for the boundary conditions: For $i = n_x - 1$ and $0 < j < n_y - 1$, we have:

$$\begin{aligned} C^{k+1}_{n_x-1,j} = C^k_{n_x-1,j} + \Delta t \frac{\mathcal{D}}{\phi}\left(\frac{C^k_{n_x-1,j} + C^k_{n_x-2,j}}{\Delta x^2} + \frac{C^k_{n_x-1,j+1} - 2C^k_{n_x-1,j} + C^k_{n_x-1,j-1}}{\Delta y^2}\right) \\ +\Delta t \frac{1}{\phi}\left(-\frac{u_{x,n_x,j}C^k_{n_x-1,j} - u_{x,n_x-1,j}C^k_{n_x-2,j}}{\Delta x} - \frac{u_{y,n_x-1,j+1}C^k_{n_x-1,j} - u_{y,n_x-1,j}C^k_{n_x-1,j-1}}{\Delta y}\right) \end{aligned} \tag{A.28}$$

For $0 < i < n_x - 1$ and $j = 0$, we have:

$$\begin{aligned} C^{k+1}_{i,0} = C^k_{i,0} + \Delta t \frac{\mathcal{D}}{\phi}\left(\frac{C^k_{i+1,0} - 2C^k_{i,0} + C^k_{i-1,0}}{\Delta x^2} + \frac{C^k_{i,1} - C^k_{i,0}}{\Delta y^2}\right) \\ +\Delta t \frac{1}{\phi}\left(-\frac{u_{x,i+1,0}C^k_{i,0} - u_{x,i,0}C^k_{i-1,0}}{\Delta x} - \frac{(u_{y,i,1} - u_{y,i,0})C^k_{i,0}}{\Delta y}\right) \end{aligned} \tag{A.29}$$

For $i = n_x - 1$ and $j = 0$

$$\begin{aligned} C^{k+1}_{n_x-1,0} = C^k_{n_x-1,0} + \Delta t \frac{\mathcal{D}}{\phi}\left(\frac{C^k_{n_x-1,0} - C^k_{n_x-2,0}}{\Delta x^2} + \frac{C^k_{n_x-1,1} - C^k_{n_x-1,0}}{\Delta y^2}\right) \\ +\Delta t \frac{1}{\phi}\left(-\frac{u_{x,n_x-1,0}C^k_{n_x-1,0} - u_{x,n_x-1,0}C^k_{n_x-2,0}}{\Delta x} - \frac{(u_{y,n_x-1,1} - u_{y,n_x-1,0})C^k_{n_x-1,0}}{\Delta y}\right) \end{aligned} \tag{A.30}$$

A.6 Analytical solution pressure

We have a partial differential equation with homogeneous boundary conditions and we apply separation of variables by substituting $r(x, y) = f(x)g(y)$ in 3.2, as follows

$$g\frac{\partial^2 f}{\partial x^2} + f\frac{\partial^2 g}{\partial x^2} = 0 \tag{A.31}$$

$$\frac{1}{f}\frac{\partial^2 f}{\partial x^2} = -\frac{1}{g}\frac{\partial^2 g}{\partial x^2} = -\lambda \tag{A.32}$$

with $\lambda > 0$ the separation constant.
From this equation we get 2 ordinary differential equations:

$$\begin{cases} \frac{d^2 f}{dx^2} = -\lambda f \\ \frac{df}{dx}(0) = \frac{df}{dx}(L) = 0 \end{cases} \tag{A.33}$$

$$\begin{cases} \frac{d^2 g}{dy^2} = \lambda g \\ \frac{dg}{dy}(0) = \frac{dg}{dy}(H) = 0 \end{cases} \tag{A.34}$$

From ODE A.33 we find, $f_n(x) = cos(\frac{n\pi}{L}x)$ with $\lambda_n = (\frac{n\pi}{L})^2$, for n = 1,2,3,...
And from ODE A.34 we find, $g_n(y) = cosh(\frac{n\pi}{H}y)$.
So we get:

$$r(x, y) = a_0 + \sum_{n=1}^{\infty} a_n cos\Big(\frac{n\pi}{L}x\Big) cosh\Big(\frac{n\pi}{H}y\Big) \tag{A.35}$$

with $a_n = 0$ for all $n \geqslant 1$ to satisfy the boundary conditions.
So we get $r(x, y) = a_0 = p(0, 0) := p_0$ and that gives:

$$p(x, y) = r(x, y) + q(x, y) = -\frac{u_0\mu}{k}x + p_0 \tag{A.36}$$

A.7 Analytical solution temperature

Here we use separation of variables by substituting $v(x,t) = f(x)h(t)$, as follows

$$\frac{1}{\alpha h}\frac{dh}{dt} = \frac{1}{f}\frac{d^2f}{dx^2} = -\lambda \tag{A.37}$$

with $\lambda > 0$ the separation constant.

To solve this equation, we first solve the spatial part of the equation:

$$\begin{cases} \frac{d^2f}{dx^2} = -\lambda f \\ f(0) = 0 \\ \frac{\gamma}{2\alpha}f(L) + \frac{df}{dx}(L) = 0 \end{cases} \tag{A.38}$$

From ODE A.38 we find, $f_n(x) = sin(\sqrt{\lambda_n}x)$ with $tan(\sqrt{\lambda_n}L) = -\frac{2\alpha\sqrt{\lambda_n}}{\gamma}$.
And for the temporal part:

$$\frac{dh}{dt} = -\lambda\alpha h \tag{A.39}$$

which gives: $h(t) = Ce^{-\lambda_n\alpha t}$

Combining these two solutions, we get

$$v(x,t) = \sum_{n=1}^{\infty} c_n sin(\sqrt{\lambda_n}x)e^{-\lambda_n\alpha t} \tag{A.40}$$

With (by using the initial condition):

$$c_n = \frac{\int_0^L \Delta T e^{-\frac{\gamma}{2\alpha}x} sin(\sqrt{\lambda_n}x)dx}{\int_0^L sin^2(\sqrt{\lambda_n}x)dx} \tag{A.41}$$

This only holds when the eigenfunctions are orthogonal. So we get:

$$T(x,t) = \sum_{n=1}^{\infty} c_n e^{-(\frac{\gamma^2}{4\alpha}+\lambda_n\alpha)t} e^{\frac{\gamma}{2\alpha}x} sin(\sqrt{\lambda_n}x) \tag{A.42}$$

A.8 Stability check

In this section we will check if the chosen numerical method for time integration (forward Euler method) is stable in equation A.18.

First define the following

$$\begin{aligned} \alpha_x &= \frac{\Delta t\alpha}{\Delta x^2} \\ \alpha_y &= \frac{\Delta t\alpha}{\Delta y^2} \\ \beta_x &= \frac{\Delta t\beta}{\Delta x} \\ \beta_y &= \frac{\Delta t\beta}{\Delta y} \end{aligned} \tag{A.43}$$

The numerical scheme becomes:

$$\begin{aligned} T_{i,j}^{k+1} = T_{i,j}^k &+ \alpha_x(T_{i+1,j}^k - 2T_{i,j}^k + T_{i-1,j}^k) + \alpha_y(T_{i,j+1}^k - 2T_{i,j}^k + T_{i,j-1}^k) \\ &-\beta_x(u_{x,i+1,j}T_{i,j}^k - u_{x,i,j}T_{i-1,j}^k) - \beta_y(u_{y,i,j+1}T_{i,j}^k - u_{y,i,j}T_{i,j-1}^k) \end{aligned} \tag{A.44}$$

Assume the solution is represented as a Fourier mode (we replaced $i = l$ to avoid confusion):

$$T_{l,j}^k = G^k e^{i(k_x l\Delta x + k_y j\Delta y} \tag{A.45}$$

Where G^k is the amplification factor after k timesteps ánd k_x and k_y are the wavenumbers in the x- and y-direction.

Substitute this expression into the numerical scheme. After substitution, the scheme becomes:

$$\begin{aligned} G = 1 + \alpha_x(e^{ik_x\Delta x} - 2 + e^{-ik_x\Delta x}) + \alpha_y(e^{ik_y\Delta y} - 2 + e^{-ik_y\Delta y}) \\ -\beta_x(u_x e^{ik_x\Delta x} - u_x) - \beta_y(u_y e^{ik_y\Delta y} - u_y) \end{aligned} \tag{A.46}$$

For the diffusion terms:

$$\begin{aligned} e^{ik_x\Delta x} - 2 + e^{-ik_x\Delta x} &= -4sin^2\left(\frac{k_x\Delta x}{2}\right) \\ e^{ik_y\Delta y} - 2 + e^{-ik_y\Delta y} &= -4sin^2\left(\frac{k_y\Delta y}{2}\right) \end{aligned} \tag{A.47}$$

We approximate the advection terms $e^{ik_x\Delta x} - 1 \approx ik_x\Delta x$, similar for $e^{ik_y\Delta y} - 1$.

Combine therms to get the amplification factor G:

$$\begin{aligned} G = 1 - 4\alpha_x sin^2\left(\frac{k_x\Delta x}{2}\right) - 4\alpha_y sin^2\left(\frac{k_y\Delta y}{2}\right) \\ -i\beta_x k_x u_x - i\beta_y k_y u_y \end{aligned} \tag{A.48}$$

For the scheme to be stable: 1. The magnitude of the amplification factor must not grow:

$$|G| \leqslant 1 \tag{A.49}$$

2. The diffusion terms contribute to decay ($\mathcal{R}(G) \leqslant 1$)) and the advection terms add oscillations ($\mathcal{S}(G)$), but shouldn't amplify $|G|$.

So the conditions that ensure stability are:

$$\begin{aligned} \Delta t &\leqslant \frac{1}{2} min(\frac{\Delta x^2}{\alpha}, \frac{\Delta y^2}{\alpha}) \\ \Delta t &\leqslant min(\frac{\Delta x}{u_x}, \frac{\Delta y}{u_y}) \end{aligned} \tag{A.50}$$

After computing this, we get that the numerical method is stable for $\Delta t_d \leqslant 0.03$.

Bibliography

[1] I. Stober & M. Jägle & T. Kohl. Optimizing scenarios of a deep geothermal aquifer storage in the southern upper rhine graben. *Geotherm Energy*, 2023.

[2] A. Hussain & B. Meulenbroek & N. Gargar & K. Wolf. Development of a well impairment model for predicting geothermal clogging. *International Journal of Heat and Mass Transfer*, 2024.

[3] L. Janssen & M.Warmoeskerken. *Transport Phenomena Data Companion.* VSSD, 2006.

[4] F. Kabus & M. Wolfgramm & A. Seibt & U. Richlak & H. Beuster. Aquifer thermal energy storage in neubrandenburg-monitoring throughout three years of regular operation. *Proceedings of the 11th International Conference on Energy Storage*, 2009.

[5] B.Meulenbroek & R.Farajzadeh & H.Bruining. Process-based upscaling of reactive flow in geological formations. *TU Delft*, 2020.

[6] International Renewable Energy Agency (IRENA). Global geothermal market and technology assessment, 2023.

[7] ThinkGeoEnergy. Geothermie nederland publishes 2022 geothermal figures, 2022.

[8] M. van den Berghe. The influence of porosity and flow rate in an aquifer on its temperature distribution. *TU Delft*, 1, october 2023.

[9] J.Veldkamp & C. Geel & E. Peters. Characterization of aquifer properties of the brussels sand. *Technical Report TEUE819001*, 2022.

[10] R. Mudde & H. van den Akker. *Fysische transportverschijnselen.* Delft Academic Press, 2014.

[11] A. A. Olsen J. D. Rimstidt, S. L. Brantley. Systematic review of forsterite dissolution rate data. *Geochimica et Cosmochimica Acta 99*, 2012.

[12] Y. K. Kharaka J. L. Palandri. A compilation of rate parameters of water-mineral interaction kinetics for application to geochemical modeling. *Geological Survey Menlo Park CA*, 2004.

[13] R. Schulz & N. Ray & S. Zech & A. Rupp & P. Knabner. Beyond kozeny-carman: Predicting the permeability in porous media. *Transp Porous Med*, 403, march 2019.

[14] M. Glinowiecka-Cox. Analytical solution of 1d diffusion-convection equation with varying boundary conditions. *Bachelor thesis, Portland State University*, 2022.

[15] G.J.M. Uffink. Dampening of fluctuations in groundwater temperature by heat exchange between the aquifer and the adjacent layers. *J. Hydrol*, 1983.